CHARACTERIZATION OF TWO-PHASE FLOW SLUG FREQUENCY AND FLOW REGIMES USING WAVELET ANALYSIS

by

© Munzarin Morshed

The thesis submitted to the

School of Graduate Studies

in partial fulfilment of the requirements for the degree of

Master of Engineering

Faculty of Engineering and Applied Science

Memorial University of Newfoundland

January 2017

St. John's Newfoundland

Abstract

The characteristics of multiphase fluid flow in pipes are useful to understand fluid dynamics encountered in the oil and gas, chemical and production industries. During the transport of different types of fluid, understanding the hydrodynamic behavior inside the pipe network is important for flow assurance. The presence of relative agitation in the interfaces and inconstant interactions among distinct phases, multiphase flow becomes a complex conveyance phenomenality in contrast to single-phase flow. This study is focused on gas/Newtonian and gas/non-Newtonian two-phase horizontal flow structure. This investigation ranges from analyzing volume fraction, pressure drop, flow regime identification, flow structure analysis, etc. This involves recognition of the two-phase flow regimes for this flow loop and validates it with the existing flow maps in the literature. In another study, slug frequency has been examined and compared with air/Newtonian and air/non-Newtonian fluid in the flow loop. Finally, wavelet packet transformation is used to decomposition pressure signals for different flow pattern.

Acknowledgement

At first, I would like to thank my supervisors Dr. Aziz Rahman and Dr. Syed Imtiaz, for their continuous help, suggestions and financial support throughout my program in the university. It was never possible to succeed without their help and support. Besides my supervisor, I would like to thank Dr. Yuri Muzychka for providing the support to use the experimental setup. I would also like to thank Dr. Aziz Rahman for providing the support in developing the experimental setup. I would like to thank Dr. Faisal Khan for organizing valuable presentations and letting me be a part of Safety and Risk Engineering group. I greatly acknowledge the funding received by School of Graduate Studies, Memorial University. I would like to thank Matt Curtis who helped me in every step towards completion of the installation process and Data Acquisition System. I also like to thank Craig Mitchel and Trevor Clark for supporting me do the experiment. I highly appreciate the help and support obtained from the Mechanical and Electronics technical service team of Memorial University led by Stephen Sooley and Bill Maloney respectively. I would like to thank Dr. Leonard Lye and his team including Moya Crocker, Colleen Mahoney and Nicole Parisi who works day and night to make things go right in the graduate office. Finally, I would like to thank my loving and supportive Husband, Al Amin and my family for encouraging me in every stage of my research program.

Co-authorship Statement

I, Munzarin Morshed, hold principal author status for all the Chapters in this thesis. However, each manuscript is co-authored by my supervisors Dr. Aziz Rahman and Dr. Syed Imtiaz, who has directed me towards the completion of this work as follows. I am the principle author and carried out the experiments. I drafted the Thesis and Co-authors assisted me in formulating research goals and experimental techniques.

Table of Contents

Abstract ii
Acknowledgement iii
Co-authorship Statement iv
Table of Contents v
List of Tables vii
List of Figures viii
List of Symbols, Nomenclature or Abbreviations xi
Chapter 1. Introduction 1
1.1 Motivation 3
1.2 Objective 3
1.3 Structure of Thesis 4
Chapter 2. Literature Review 5
2.1 Flow Map 5
2.2 Slug Frequency 10
2.3 Signal Analysis 15
2.4 Fluid Properties 18
2.5 Conclusion 22
Chapter 3. Experimental Setup 23
3.1 Introduction 23
3.2 Different Components of the Setup 24
3.3 Fluid Properties 34
Chapter 4. Flow Map 43
4.1 Introduction 43
4.2 Flow Regimes 44
4.2.1 Stratified/Wavy flow 45
4.2.4 Annular Flow 48
4.3 Flow Map for Horizontal Flow 49

4.4 Conclusions....52
Chapter 5. Slug Frequency....53
5.1 Introduction....53
5.2 Slug Velocity....54
5.3 Slug Frequency....56
5.4 Experimental Results....60
5.4.1 Air/Newtonian Two-phase flow....60
5.4.2 Air/non-Newtonian Two-phase flow....67
5.5 Conclusion....73
Chapter 6. Signal Analysis....74
6.1 Introduction....74
6.2 Wavelet Analysis....76
6.2.1 Contentious Wavelet Transform (CWT)....77
6.2.2 Discrete Wavelet Transform (DWT)....77
6.3 Wavelet Packet Analysis of the Experimental Data....84
6.3.1 Wavelet Spectrum Analysis....84
6.3.2 Wavelet Entropy Analysis....86
6.4 Conclusion....91
Chapter 7. Conclusion....92
7.1 Future Recommendation....93
Bibliography....95

List of Tables

Table 3.1: Pump Specifications. 25
Table 3.2: Types of non-Newtonian Fluid 35
Table 3.3: Specification of 0.1% Xanthan gum 42
Table 5.1: Experimental Parameters 60

List of Figures

Figure 2.1: Mandhane et al. (1975) (adapted) flow map for Horizontal gas/Newtonian two-phase flow. 6
Figure 2.2: Taitel & Dukler (1976) (adapted) flow map for gas/Newtonian horizontal flow. 7
Figure 2.3: Taitel & Dukler (1976) (adapted) flow map for gas/Newtonian horizontal flow using Lockhart & Martinelli (1949) parameter X. 8
Figure 2.4: Chhabra & Richardson (1984) (adapted) flow regime map for gas/non-Newtonian horizontal flow....9
Figure 2.5: Time-independent fluid flow behaviour. 20
Figure 2.6: Time-dependent fluid behaviour. 21
Figure 3.1: Schematic of Experimental Setup (Horizontal Test Section)....24
Figure 3.2: TB Wood AC Inverter. 25
Figure 3.3: Liquid Reservoir Tank 26
Figure 3.4: Omega FTB-730 Turbine Flowmeter 27
Figure 3.5 Omega FLR6750D air flowmeter. 27
Figure 3.6: Air flow lines....28
Figure 3.7: Omega PX603100G pressure sensor and the calibration curve. 29
Figure 3.8: Control valve for the air flow. 30
Figure 3.9: National Instrument Data Acquisition System....31
Figure 3.10: Pressure Relief Valve....32
Figure 3.11: Snubber for the pressure transducer....33
Figure 3.12: Viscosity vs shear rate curve for 0.1% Xanthan gum solution(adapted from CP Kelco Xanthan gum book, page-5). 37
Figure 3.13: Viscolite VL 700 viscometer. 38
Figure 3.14: Viscosity versus shear rate curve for 0.1% and 0.2% Xanthan gum from the experimental data....40
Figure 3.15: Shear stress versus shear rate curve for 0.1% Xantahn gum solution. 40
Figure 4.1: Different flow regime for gas/Newtonian flow. 46

Figure 4.2: Different flow regime for gas/non-Newtonian flow. [Adapted from Dziubinski et al. (2004)] 46
Figure 4.3: Different part of a Slug unit; adapted from Dukler & Hubbard (1975)..... 48
Figure 4.4: Comparison of the Taitel & Dukler (1976) (adapted) flow map with experimental data for horizontal gas/Newtonian flow. 49
Figure 4.5: Comparison of the Mandhane et al. (1974) (adapted) flow regime map with experimental data obtained for horizontal gas/Newtonian flow. 50
Figure 4.6: Comparison of the (Chhabra & Richardson 1984) (adapted) flow regime map with experimental data obtained for horizontal gas/non-Newtonian flow. 51
Figure 5.1: Effect of liquid superficial velocity on slug frequency for air/water flow..... 60
Figure 5.2: Effect of gas superficial velocity with slug frequency for air/water two-phase flow. 61
Figure 5.3: Slug frequency vs mixture velocity for air/water flow. 62
Figure 5.4: Slug frequency versus Froude number for air/water flow. 63
Figure 5.5: Regression of Slug frequency by Froude number graph and the strength of the model R^2=88.1%. 64
Figure 5.6: Experimental slug frequency for air-water system compared with the predictions model of Gregory & Scott (1969) correlation. [R^2=73.8%] 65
Figure 5.7: Experimental slug frequency for air-water system compared with the predictions model of Zabaras et al. (2000) correlation. [R^2=60%] 66
Figure 5.8: Effect of liquid superficial velocity with slug frequency for air/non-Newtonian flow. 67
Figure 5.9: Effect of gas superficial velocity with slug frequency for air/non-Newtonian flow. 68
Figure 5.10: Slug frequency vs mixture velocity for air/non-Newtonian fluid flow. 69
Figure 5.11: Slug frequency versus Froude number for Air/Xanthan gum solution. 71
Figure 5.12: Experimental slug frequency for air-Xanthan gum system compared to the predictions by Gregory & Scott (1969) correlation where R^2=74.6% 72
Figure 6.1: Wavelet transformation of sine wave. 76

Figure 6.2: Multiple level Discrete Wavelet analysis.....78
Figure 6.3: Wavelet packet analysis decomposition tree.....81
Figure 6.4: The steps of wavelet decomposition for different flow pattern identification. 83
Figure 6.5: Spectrum for Slug flow at different flow condition. 85
Figure 6.6: Spectrum for bubbly flow in different flow condition.....85
Figure 6.7: Change of wavelet entropy with gas volume fraction for gas/Newtonian fluid. 87
Figure 6.8: Change of wavelet entropy with gas volume fraction for gas/non-Newtonian fluid.....88
Figure 6.9: Change of wavelet entropy with Gas to Liquid Ratio for gas/Newtonian flow. 89
Figure 6.10: Wavelet entropy flow map for gas/Newtonian flow.....90
Figure 6.11: Wavelet entropy flow map for gas/non-Newtonian flow.....90

List of Symbols, Nomenclature or Abbreviations

v_l^s	Superficial Liquid Velocity, m/s
v_g^s	Superficial Gas Velocity, m/s
v_l	Liquid Inlet Velocity, m/s
v_g	Gas Inlet Velocity, m/s
ρ_w	Water Density=996 kg/m^3
μ_w	Water Viscosity 0.999 mPa.s at 20℃
l_p	Pipe Length, m
d	Pipe Diameter, mm
v_m	No-Slip Mixture Velocity, m/s
λ	Liquid Volume Fraction
f_s	Slug Frequency, 1/s
v_G	True Average Gas Velocity in Multiphase Flow, m/s
N_{f_s}	Froude Number
v_m^0	Minimum Slug Frequency in The Graph=6 m/s
v_{m_n}	No-Slip Mixture Velocity for Non-Newtonian Fluid, m/s
f_{sn}	Slug Frequency for Non-Newtonian Fluid, 1/s
$N_{f_{sn}}$	Froude Number for Non-Newtonian Fluid

v_{l_n}	Non-Newtonian Liquid Inlet Velocity, m/s
Re_w	Water Reynolds Number
Re_n	Non-Newtonian Reynolds Number
n	Power Law Index
m *or* k	Power Law Index
ρ_n	Non-Newtonian Density=1002 kg/m^3
γ_{yx}	Shear Rate, 1/s
σ	Shear Stress, Pa
μ_n	Apparent Viscosity, cP
x	Signal
$W(j, k)$	Wavelet Transform
$\Psi_{jk}(x)$	Wavelet Base
k	Wavelet Level
j	Wavelet Scales
$\varphi_{j,k}$ (x)	Scale Function

Chapter 1. Introduction

Multiphase flows are considered as complicated flow phenomena over single flow. There are still essential features of multiphase flow whose modeling outcome are contentious and structural explanation are still unexplored. The most common type of multiphase flow is the two-phase gas/liquid flow in almost all chemical, petroleum and production industries. Different forms of flow pattern may be observed when two or more than two phases flow simultaneously. Sometimes experiential investigations are challenging when in the pipe cross section, there is unpredictable turbulent flow structure generating highly asymmetric volume distribution. This kind of unstable flow condition complicate the measurement process sometime it become challenging to capture the actual flow condition. There are also instances where the existing theoretical solution or experimental results cannot describe the certain physical properties such as in-situ volume fraction, flow structure, flow mechanism and so on.

The fusion of distinctive phases (such as liquid, gas and solid) flowing through a pipeline is called multiphase flow. The multiphase flow properties are much more diverse and complicated compared to that of single phase flow. The flow regimes or the flow pattern are one of the major aspect of multiphase flow. The flow structural distribution of different phases in the pipe, is known as flow pattern or flow regime. The flow regime depends on the inertia force, buoyancy force, flow turbulence and surface tension which are altered by the fluid properties, flow rates, pipe diameter and pipe predilection. This study is only focused on gas/Newtonian and gas/non-Newtonian two-phase horizontal flow analysis. Different forms of flow pattern may be observed when two phases gas/Newtonian and

gas/non-Newtonian flow simultaneously. Some of the common flow patterns are: stratified flow, where the liquid and gas phase are separated and the gas flows on the top as its lighter than liquid; bubbly flow, where there is dispersion of small sized bubbles with liquid; Slug flow in which each gas bubbles form a large slug shape that is often a bullet shape; and annular flow where liquid flow as a film on the wall of the pipe. For gas/Newtonian and gas/non-Newtonian flow there are several flow maps to predict the flow patterns. Taitel & Dukler (1976) flow map and Mandhane et al. (1975) flow map for gas/Newtonian flow and Chhabra & Richardson (1984) flow map for gas/non-Newtonian are the most frequently used flow maps.

Experimental research in multiphase flow phenomena involves different types of sensors to capture the in-situ flow structure and flow characteristic. The most common sensors are pressure fluctuation sensor, differential pressure sensor, gamma-ray tomographic sensor and particle image velocimetry (PIV). The fluctuation of the signals are measured from the sensors. It is challenging to predict the flow characteristics form the output signal. This is where the needs of time domain or frequency domain signal analysis methods come in. Fast Fourier Transform, power spectral density function (PSD), wavelet transform, Hilbert-Huang transform, neural network approach, etc. are the most common signal analysis methods. Among them wavelet analysis has been the most popular time domain signal analysis method which decomposes the signal and can identify the behavior and parameter of the signal.

The uniqueness of this study, is that the experiments has been performed in a setup with 73.66 mm ID and approximately 19 m flow loop. This flow loop has horizontal, vertical

and inclined test section connected. However, this study is focused on horizontal flow aspects and gas/Newtonian and gas/non-Newtonian flow characteristics. Another major focus of this thesis is to understand the characteristics of pressure signal based on different flow regime and suggesting a convenient way to decompose the signals to identify different flow regime based on pressure signal attributes.

1.1 Motivation

Slug flow is the most frequent two-phase flow phenomena experienced in the horizontal or near horizontal pipeline in the practical field. Multiple operational problems such as pipeline network instability, damaging equipment by high-pressure fluctuation or vibration of the system are caused by slug flow. This can also be termed as water hammering effect. Therefore, in multiphase flow, slug flow and slug frequency analysis has been one of the major research interest.

1.2 Objective

The goal of the thesis is to characterize 2-phase Newtonian/gas and non-Newtonian/gas flow using a Data Acquisition System (DAQ) to collect data from the different pressure transducer and flow transmitter installed in the flow loop. This study focuses on slug frequency analysis in a 73.66 mm I.D. horizontal pipe using gas/Newtonian and gas/non-Newtonian two-phase flow. Moreover, flow maps are reconstructed and validated with the existing literature to identify the two-phase flow regimes for this experimental setup. Lastly, characterization of pressure signals using time and frequency domain analysis (i.e. Wavelet Transformation). The pressure signals are decomposed using wavelet packet

transform to get an understanding of the change of pressure fluctuation based on norm entropy with the change of different flow regimes.

1.3 Structure of Thesis

The thesis is organized as follows: Chapter 2 provides an overview of the two-phase flow maps, slug frequency, wavelet packet transformation and recent development in this sector. Chapter 3 presents the design and components used in the experimental setup. Chapter 4 discusses the flow maps for different flow regimes. Chapter 5 provides the slug frequency analysis for both gas/Newtonian and gas/non-Newtonian two-phase flow. Chapter 6 shows the pressure fluctuation analysis using wavelet packet transformation for bubble and slug flow regimes. Finally, chapter 7 provides the concluding discussion of this thesis and recommendation of future research.

Chapter 2. Literature Review

2.1 Flow Map

Flow regime analysis is a significant part of the multiphase flow analysis. In order to estimate the hydrodynamic feature of multiphase flow, it is necessary to have knowledge about the actual flow pattern under specific flow condition. Multiphase flow regime implies gas/liquid, gas/liquid/solid or liquid/solid flow together through a pipeline system. In this study, only two phase gas/liquid flow characteristics have been analyzed. When two phases flow through a pipeline, different types of interfacial distribution can form. Some of the common distribution are: bubbly flow, where there is dispersion of small sized bubbles with liquid; slug flow in which each gas bubbles form a large slug shape that is often a bullet shape; stratified flow, where the liquid and gas phase are separated and the gas flows on the top as its lighter than liquid; and annular flow where liquid flow as a film on the inner surface of the pipe.

These flow patterns occur for certain combination of gas/liquid flow rate. After doing many research gas/Newtonian flow pattern map has been advanced to predict the flow patterns. The flow map tries to predict the different types of flow regions. Mandhane et al. (1975) flow map have been the most frequently used flow map for gas/Newtonian flow. Mandhane et al. (1975) used 1400 experimental data from AGA-API two-phase flow data bank and developed this flow map for horizontal two-phase flow.

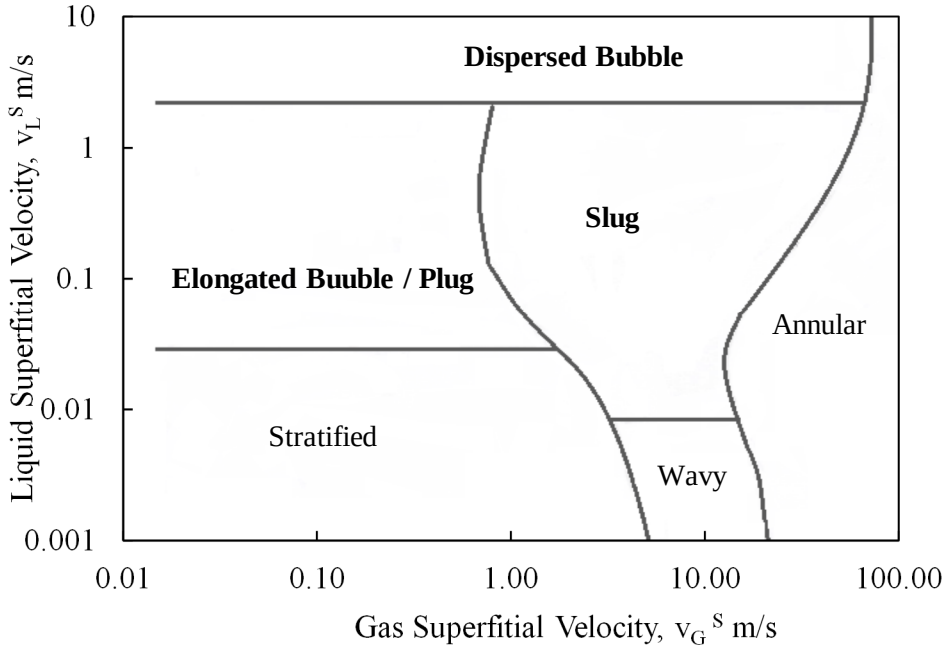

Figure 2.1: Mandhane et al. (1975) (adapted) flow map for Horizontal gas/Newtonian two-phase flow.

The flow map shown in Figure 2.1, is a function of superficial liquid velocity plotted in contrast to superficial gas velocity and the boundary line are drawn to separate different flow regime.

Taitel & Dukler (1976) flow map has been another popular and commonly used flow map. The flow maps demonstrate the functional relationship of superficial liquid velocity plotted in contrast to superficial gas velocity as shown in Figure 2.2.

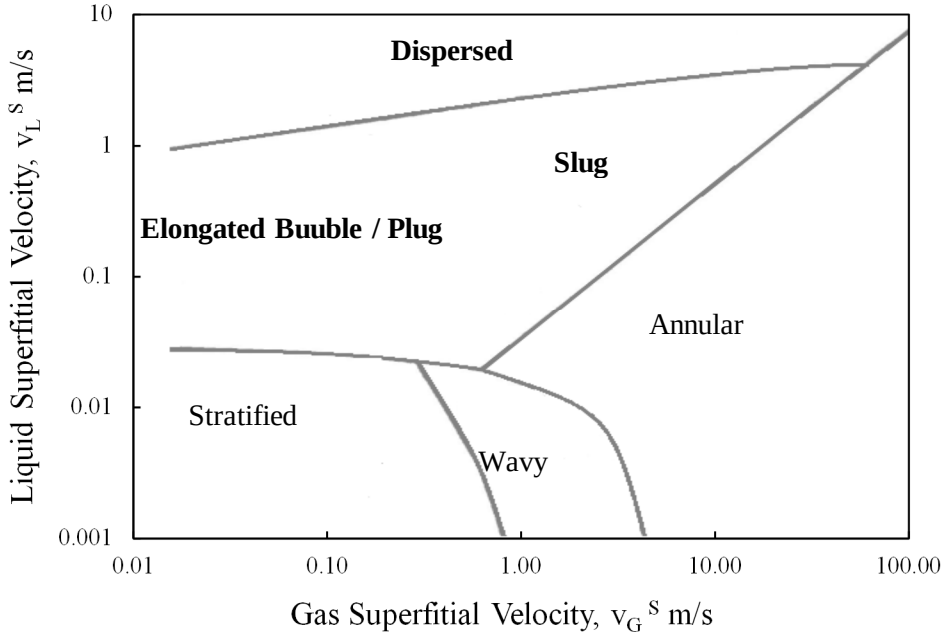

Figure 2.2: Taitel & Dukler (1976) (adapted) flow map for gas/Newtonian horizontal flow.

Another flow map was developed where Lockhart & Martinelli (1949) parameter X and another dimensionless parameter k which were used in the horizontal and vertical axis (shown in Figure 2.3). The Taitel & Dukler (1976) flow map was computationally challenging and based on the theoretical model. Besides that, Lockhart & Martinelli Parameter X required pressure drop value to calculate whereas, the above flow map in Figure 2.2 requires only superficial liquid and gas velocity.

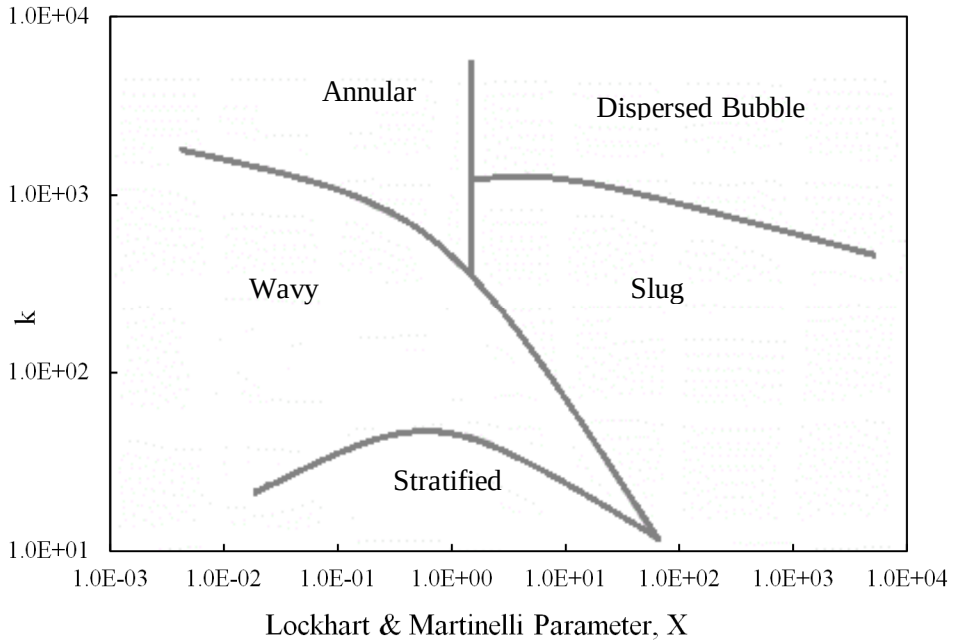

Figure 2.3: Taitel & Dukler (1976) (adapted) flow map for gas/Newtonian horizontal flow using Lockhart & Martinelli (1949) parameter X.

Here, k parameter is a function of water and gas density, velocity, water viscosity and pipe diameter. The formula of X and k parameters are shown below.

$$k = \sqrt{\frac{\rho_w}{\rho_w + \rho_g}} \frac{v_g^s}{\sqrt{dg\,cos\alpha}} \left[\frac{dv_l^s}{\mu_w}\right]^{0.5} \tag{2.1}$$

$$X = \sqrt{\left|\frac{dP_l}{dl_p}\right| \Big/ \left|\frac{dP_g}{dl_p}\right|} \tag{2.2}$$

Chhabra & Richardson (1984) developed a flow pattern map for air/non-Newtonian flow. The map was prepared using Mandhane et al. (1974) horizontal flow pattern map as shown in Figure 2.4. The flow map was verified with 3700 data point of gas/non-Newtonian shear-thinning air/liquid two flow where the map predicted 70% of the flow regimes. Particulate suspension of China clay, limestone, coal-aqueous polymer solution has been used as the shear-thinning liquid for the experimental data points. The liquid flow regime velocity range was 0.021 m/s - 6.1 m/s, gas velocity range was 0.01m/s – 55m/s and 6.35 mm to 207 mm I.D pipe. However, there was not enough data for annular and slug flow to verify Chhabra & Richardson (1999) flow map.

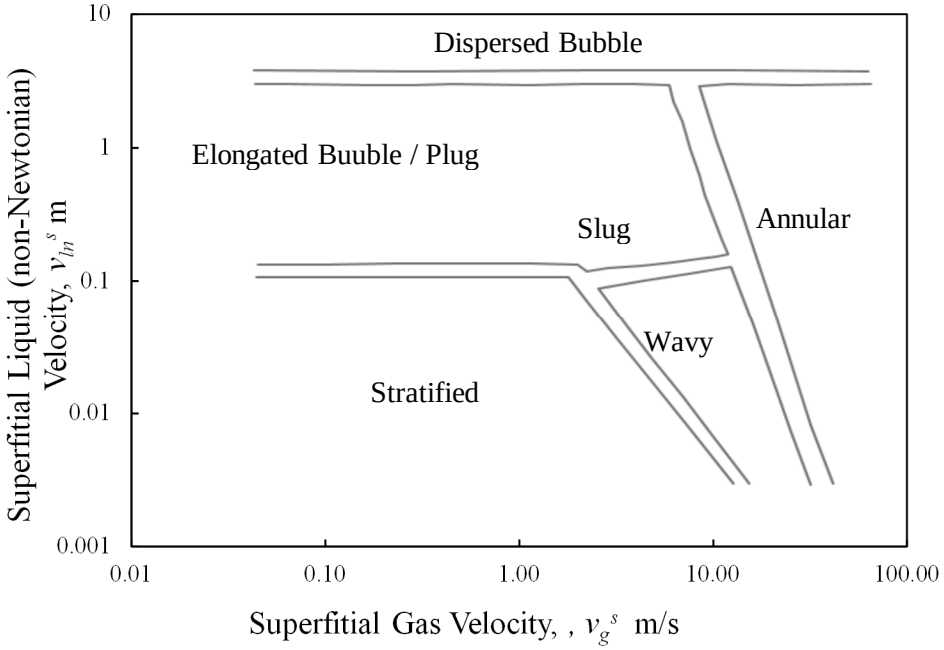

Figure 2.4: Chhabra & Richardson (1984) (adapted) flow regime map for gas/non-Newtonian horizontal flow.

2.2 Slug Frequency

Slug flow is one of the most prevalent flow phenomena in petroleum, production and chemical industries. Slug flow is a state of flow which can create an unwanted situation like pipeline mutability or damage the equipment due to its hammering effect and create a lot of vibration. This water hammering effect is also called slug frequency. In two phase flow when the liquid slugs are separated by bullet shaped gas pockets it is slug flow and slug frequency is the number of slug passing a specific point with time. There are many studies which focused only on slug flow regime and tried to understand the flow structure and characteristics of this flow regime.

The most used slug flow model was described by Hubbard & Dukler (1966) where air-water slug frequency was determined. Gregory & Scott (1969) also used Hubbard & Dukler (1966) slug flow model to determine slug velocity and slug frequency for their experiment. In this study, Carbone dioxide-water was used in 19.05 mm I.D. pipe to create two-phase slug flow. Two strain gauge pressure transducer has been used to measure the pressure. The slug frequency was measured by visual observation and measuring the pressure pulses recorded from the pressure gauge. Gregory & Scott (1969) showed in their experimental data that there was a minimum value of slug frequency in the slug frequency versus slug velocity (or mixture velocity) graphs for air/water flow. After observing the flow pattern, Gregory & Scott (1969) suggested a velocity dependent empirical Equation (2.3) where slug frequency was correlated with a form of Froude number.

$$N_{f_s} = \frac{v_l}{gd}\left[\frac{(v_m^0)^2}{v_m} + v_m\right] \tag{2.3}$$

Here, v_m^0 was taken 6 m/s. From slug frequency versus slug Froude number graphs Gregory & Scott (1969) achieved the following Equation (2.4) below.

$$f_s = 0.0157\left(N_{f_r}\right)_{slug}^{1.20} \sec^{-1} \tag{2.4}$$

From Equation (2.4), Gregory and Scott (1969) developed a slug frequency correlation based on his liquid-gas two-phase flow experimental data which is shown in the Equation (2.5).

$$f_s = 0.0226\left[\frac{v_l^s}{gd}\left(\frac{19.75}{v_m} + v_m\right)\right]^{1.2} \tag{2.5}$$

Here, $v_m \; and \; v_l^s$ is the mixture velocity and superficial liquid velocity of liquid and gas in m/s. Therefore, this slug frequency can be combined with Froude number established on liquid superficial velocity. Greskovich & Shrier (1972) reorganized Gregory & Scott (1969) correlation.

$$f_s = \left[0.0425\frac{v_l^s}{v_m}\left(\frac{2.02}{d} + \frac{v_m^2}{gd}\right)\right]^{6/5} \tag{2.6}$$

Heywood & Richardson (1979) determined liquid volume fraction for air-water two-phase flow applying the gamma-ray technique in 41.91 mm I.D. horizontal pipe. To achieve liquid volume fraction, they used power spectral density function and probability density function. These features are also helpful to determine different slug flow characteristics such as the value of average film and slug volume fraction, average slug frequency and average slug length. The slug frequency correlation was determined by curve fitting the data. In the Equation (2.7) λ is the liquid volume fraction and $\lambda = v_l^s/(v_l^s + v_g^s)$ and d is the pipe diameter in mm.

$$f_s = \left[0.0462\,\lambda\left(\frac{1}{0.0126d} + \frac{v_m^2}{gd}\right)\right]^{1.02} \tag{2.7}$$

Zabaras (1999) described different proposed model and correlation of slug frequency and compared the existing data with the predicted methods. A modification version of Gregory & Scott (1969) correlation was suggested based on 399 data points with lowest standard deviation and average absolute error for both horizontal and inclined pipe flow. The correlation is shown the Equation (2.8), where θ is the inclination angle. The experiment was done with air and water.

$$f_s = \left[0.0425\frac{v_l^s}{gd}\left(\frac{1}{0.0506v_m} + v_m\right)\right]^{6/5}[0.836 + 2.7\,sin^{0.25}\,\theta] \tag{2.8}$$

Shea et al. (2004) correlation described as a function of pipe length. This correlation is based on curve fitting of field and laboratory data instead of theoretical analysis. In this equation, it is also shown that the slug frequency is inversely dependent on the pipe length l_p, which does not agree with the other theoretical analysis. According to Al-Safran (2009), OLGA 2000 slug tracking model had some time delay problem between two slugs, to solve this issue Shea et al. (2004) correlation was initially used. The slug frequency equation is shown below.

$$f_s = 0.47\left[\frac{(v_l^s)^{1.5}}{l_p^{1.1}d^{2.4}}\right]^{0.5} \tag{2.9}$$

Where, v_l^S is the superficial liquid velocity in m/s, d is the pipe diameter in mm and l_p is the pipe length in m. Equation (2.9) used the pipe length, which could be questionable for long distance transmission system with hilly condition.

Rosehart et al. (1975) described slug frequency and slug velocity for air/non-Newtonian fluid flow. The experiment was performed in 25.4 mm I.D. horizontal tube with three different polymer solution, which was CMC (Carboxymethyl cellulose), Polyhall 295 and Carbpoll 941. One of the major assumptions for slug velocity of slug flow model for both air/Newtonian and air/non-Newtonian fluid was that the liquid slug front flows at the maximal of the gas velocity, so the average velocity ratio would be almost the same for all system. Rosehart et al. (1975) verified and proved this assumption in this study. For slug frequency analysis

Rosehart et al. (1975) used Gregory & Scott (1969) method shown in Equation (2.5), but got different constant values for various types of gas-liquid viscosity combinations and couldn't obtain a generalized correlation for all the polymer system. He also concluded that when the Polyhall solution concentration increases slug frequency decreases.

Otten & Fayed (1977) analyzed slug velocity and slug frequency for both air/water and air/non-Newtonian horizontal slug flow. In this study, Carbopol 941 solution was used as a non-Newtonian fluid and the experiment was done in 25.4 mm I.D. horizontal pipe with 4.9 m test section. Otten & Fayed (1977) concluded that the slug frequency is a function of drag and proportional to Carbopol concentration (when it is less than 40mg/L). The study validated Rosehart et al. (1975) work relating Carbopol concentration with slug frequency. It was found that the slug frequency increases with increased liquid concentration.

Picchi et al. (2015) described a slug frequency equation which considers the rheology of the shear-thinning fluid. The experiments were done in 22.8 mm I.D. horizontal and slightly inclined glass pipe with different concentration of Carboxymethyl Cellulose (CMC) solutions. The superficial velocity was from 0.05 m/s to 1.4 m/s for CMC-water solutions and 0.1 m/s to 2 m/s for gas superficial velocity. Picchi et al. (2015) slug frequency equation are the modified version of Gregory & Scott (1969) correlation considering the rheological properties of the shear-thinning fluid .

$$f_s = 0.0448 \left[\frac{v_{l_n}}{gd} \left(\frac{32.2014}{v_{m_n}} + v_{m_n} \right) \right]^{.88} n^{-2.85} \left(\frac{Re_n}{Re_w} \right)^{.07} \qquad (2.10)$$

Where, $Re_w = \frac{\rho_w v_l^s d}{\mu_w}$ is the water Reynolds number and $Re_n = \frac{d^n v_{l_n} \rho_n}{m 8^{n-1} \left(\frac{1+3n}{4n}\right)^{n-2}}$ is the power-law fluid Reynolds number at superficial condition, where n and m is the fluid behavior index.

From the above discussion, it has been seen that Gregory & Scott (1969) slug frequency correlation has been the most popular and frequently used slug frequency correlation. In this study, this correlation also used to validate the experimental results.

2.3 Signal Analysis

The multiphase flow widely exists in different kind of industries and gas/liquid two-phase has been the most common phenomena which create a complex flow structure while flowing through the pipeline. In order to design an optimized system in the industries, flow pattern identification knowledge is essential for avoiding the unstable situation and maximizing the use of the system. Visual identification has been the easiest way of identifying different flow patterns, but it is not possible for a complex, high-pressure or high-temperature system where using transparent pipes can be inconvenient. This problem can be resolved by using sensors such as pressure sensor, tomographic sensor, electrode conductive sensor, particle image velocimetry (PIV) sensor, gamma ray sensor, etc. Most of these sensors give different types of signals as measured outputs and analyzing the signal is also a major challenge. Fast Fourier Transform, neural network approach, wavelet transform, power spectral density function, Hilbert-Huang transform are the most commonly used signal analysis methods based on a time domain or frequency domain. Among different types of signals, pressure signal analysis is the most common type of

signal analysis and numerous two phase flow experimental pressure signals have been analyzed throughout the years using wavelet transform and some of them are discussed below.

For identifying two-phase flow regime Elperin and Klochko (2002) used wavelet transformation to process time series differential pressure fluctuation measured through venturi meter. The experiment has been done in a multiphase flow facility with vertical test section. In the paper, to identify flow regimes, Daubechies' level 4 (db4), eight-level wavelet transform energy distribution has been used. From this study, it has been concluded that the energy of the bubble flow is concentrated in the small-time scale which represents the randomly distributed moving gas bubbles. For annular flow, the fluctuation decreased. The smaller scaled and medium scaled peaks wavelet spectrum characteristics show slug and churn flow regime.

Park & Kim, (2003) have done wavelet packet transform to analyze pressure fluctuations in a bubble column for air (0.02-0.1 m/s) and water (0-.010 m/s) flow. This experiment was conducted in a bubble column apparatus with a 376 mm I.D. vertical column test section and differential pressure transducer. In the experiment pressure fluctuation for bubbly and churn-turbulence flow has been studied. In this study, power spectral density function of the pressure signal also analyzed and the Fourier basis localized only the frequency and couldn't reveal time localization. On the other hand, wavelet transforms don't have this disadvantage. From the wavelet packet table and spectrogram analysis of the signals, it has been observed that the energy content in the lower frequency ranges increases with the

increased bubble size. Moreover, the churn-turbulent flow regime has coarser scale and frequencies than the bubble flow regime.

Fan et al. (2013) used multiresolution wavelet transform to analyze conductance fluctuation signal of different two-phase flows in a vertical pipe. In this study wavelet entropy of the conductance fluctuation signal has been calculated to differentiate between bubble, slug and churn flow and a wavelet entropy versus gas flow rate flow map also developed for vertical upward flow. The pipe diameter of this vertical upward dynamic experiment was 125 mm with eight electrode conductance sensor measurement which consists of a pair of excitation electrode and two cross-correction electrodes for flow measurement. The water flow range was 1-12 m^3/h and gas flow range was 0.5-140 m^3/h with the 400 Hz sampling frequency. In the wavelet analysis, DB4 and scale 8 decompositions have been done to find low-frequency coefficients based on wavelet entropy theory and then wavelet entropy of the conductance fluctuation signal has been analyzed. In this study, it is concluded that the wavelet entropy has a significant effect on the flow characteristics and different types of entropy range has been achieved for different kinds of flow.

De Fang et al. (2012) also used wavelet analysis to understand the gravity differential pressure fluctuation signal perpendicular to the horizontal flow of different flow patterns and the flow pattern transition of gas/liquid two-phase flow in the horizontal pipe. In this study, the experiment has been done in the low-pressure gas/liquid two-phase flow experimental setup, where the test section has 50 mm I.D. pipe with a split-type high-frequency differential pressure transducer in 1 kHz. In the experiment, the water velocity

range has been around 0-0.55 m/s and the gas flow rate has been around 0-180 m^3/h and Haar wavelet with six level has been used to decompose the pressure signal. The energy value has been obtained for each scale. The bi-spectral analysis of experimental data of the gravity differential pressure signal also has been done here to get a clear view of the interphase energy. From this study, it has been observed that when gas flow rate increased in liquid flow, the interphase force starts increasing and the energy value also increased, which state that the wavelet energy is sensitive to the laminar to annular flow transition.

Sun et al. (2013) used wavelet packet energy entropy to recognize gas/liquid flow pattern and constructed a flow pattern map. In the study, energy entropies of vortex-induced pressure signal across a bluff body has been analyzed using the wavelet packet transform. For this experiment 50 mm I.D. pipe has been used with a prismatic bluff perpendicular to the fluid flow to generate vortex at a b=w/D=0.28 blockage ratio. To acquire the differential pressure signal data a dynamic piezo-resistive sensor with 1kHz sample rate has been used. Bubble, plug, slug and annular flow has been observed through experiments for air/water flow. The pressure signals have been analyzed using level four and four scales Daubechies based wavelet (db4) which provided sixteen wavelet packet coefficients. In this analysis, 1-D wavelet packet transformation has been used to decomposed the experimental pressure signal and determine the norm entropy of the signal for different flow patterns.

2.4 Fluid Properties

In this study, two types of fluid have been used, Newtonian fluid and non-Newtonian fluid. These two fluid are mainly differed based on their viscosity properties. Viscosity is the

measure of opposing the deformation by shear, in another word it is the ratio of the shear stress $\sigma = \frac{F}{A}$ and velocity gradient $\frac{dv}{dy}$. Newtonian fluid velocity gradient can be expressed as shear rate $\dot{\gamma}_{yx}$ which is normal to the force and shown in the Equation (2.12).

$$\mu = \frac{F}{A}\left(-\frac{dv}{dy}\right)^{-1} = \sigma\left(\dot{\gamma}_{yx}\right)^{-1} \tag{2.11}$$

Whereas, apparent viscosity μ_n is also the ratio of the shear stress and shear rate and rely upon the shear rate. Apparent viscosity is constant and equal to the fluid viscosity for a Newtonian fluid, but the number changes for non-Newtonian fluid.

The Newtonian fluid viscosity is constant which means shear stress and shear rate is proportional and the viscosity slope is equal to 1 and dependent on material and its temperature.

For non-Newtonian fluid, the shear stress versus shear rate slope become a curved line and does not shows a constant value and depends on shear rate, flow geometry, etc. There are three types of non-Newtonian fluids based on apparent viscosity. They are, time independent fluid, time-dependent fluid and viscoelastic fluid.

Time-Independent Fluid

Time-independent fluid is only depended on share rate and temperature. For this fluid, the shear rate is arbitrated only by the amount of shear stress at that instant and at that point. These types of fluid can be subdivided into three categories. Firstly, with shear-thinning

fluid apparent viscosity decreases with increment of shear rate. Secondly, with shear-thickening fluid apparent viscosity increase with rising shear stress. Lastly, viscoplastic fluid, which must overcome a yield stress before flowing when stress is applied and the flow curve never go through the origin (Chhabra & Richardson 1999). These three types of time-independent fluid characteristics are shown in an approximately linear scale flow curve in Figure 2.5.

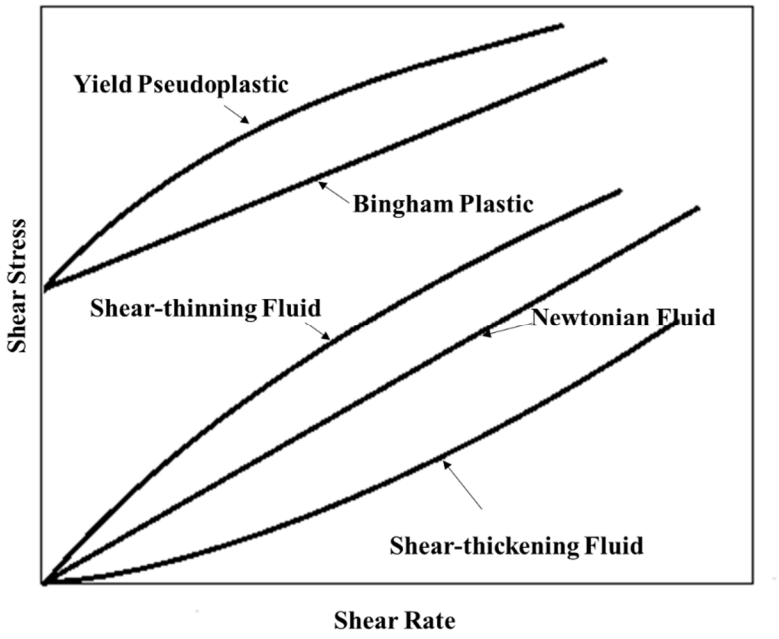

Figure 2.5: Time-independent fluid flow behaviour.

Time-Dependent Fluids

Time-dependent fluids are those fluids with which apparent viscosity changes with time while shear stress is applied. Time depended fluids are divided into two categories. Firstly, thixotropy in which apparent viscosity decrease with the time at a constant shear rate. If an experiment is done using thixotropic fluid and the shear rate is undeviatingly rise at a consistent scale from zero to the largest value and then diminished at the same proportion to zero, then a hysteresis loop will develop which is shown in Figure 2.6. Another type of time- dependent fluid is rheopexy or negative thixotropy. These types of fluid act contrary to thixotropy and apparent viscosity rises with time at a consistent shear rate. Rheopectic fluid also shows an hysteresis loop but it is an inverted hysteresis loop shown in Figure 2.6 (Chhabra & Richardson 1999).

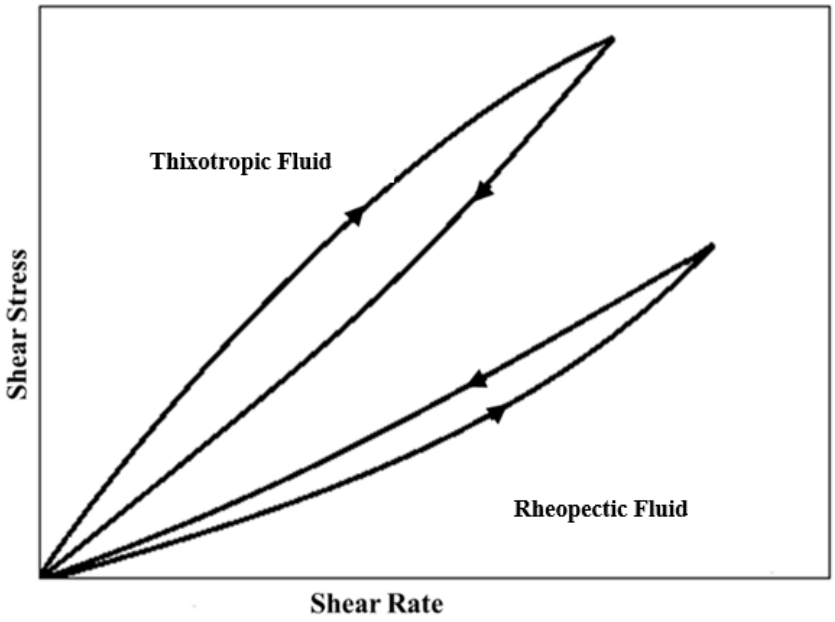

Figure 2.6: Time-dependent fluid behaviour.

Viscoelastic fluid

Another type of non-Newtonian fluid is viscoelastic fluid, which has the elastic properties. When a material deforms under stress and regains its original form after removing the stress is called elastic material. Many material exhibits both viscous and elastic properties under certain condition. Many materials like melted polymer or soap solution shows visco-elastic properties under some condition when it can reserve and redeem shear energy.

In this study, water is used as the Newtonian fluid. For non-Newtonian fluid, time-independent shear thinning 0.1% Xanthan gum solution is utilized in the experiments.

2.5 Conclusion

From the previous discussion, it is evident that many research has been accomplished in multiphase flow analysis, especially using two-phase flow. This investigation ranges from analyzing volume fraction, pressure drop, flow regime identification, flow structure analysis, etc. Our focus in this study is to analyze the horizontal flow regime map using experimental data. This involves recognition of the two-phase flow regimes for this flow loop and validates it with the existing flow maps in the literature. In another study, slug frequency has been examined and compared with air/Newtonian and air/non-Newtonian fluid in the flow loop. Finally, pressure signal decomposition has been done for bubble and slug flow using wavelet packet transformation.

Chapter 3. Experimental Setup

3.1 Introduction

The experiments were performed in a flow loop system which has a horizontal, vertical and inclined section. However, in this paper, we are only considering the 4-meter horizontal section as our test section. The experimental setup is 60-meter-long closed cycle system for water and open cycle system for air. The liquid is pumped by a 5 HP pump that creates the required large volume water flow through DN80 or 2.9 I.D. PVC clear pipes. The airline of the flow loop had DN15 and DN25 mild steel pipe which supplies air from lab air supply at 670 kPa (100 psi) shut-in pressure. It also includes a DN 25 ball check valve just before the air and the liquid mixing zone to prevent any liquid from entering the air pipeline. There are two Omega PX603-100G5V pressure transducers with a range of 0 to 100 psi in the 2-meter long horizontal test section. There are some specific experimental conditions used for this setup. The air flow range is about 85 L/min to 3300 L/min (Approx.), the water flow range is almost 250 L/min to 850 L/min. At this range the experimental setup mostly gives slug flow for two-phase flow, it also gives bubble flow and wavy flow at some range. Figure 3.1 presents a schematic representation of the experimental setup. For this study, both gas/Newtonian and gas/non-Newtonian fluid flow cases have been considered

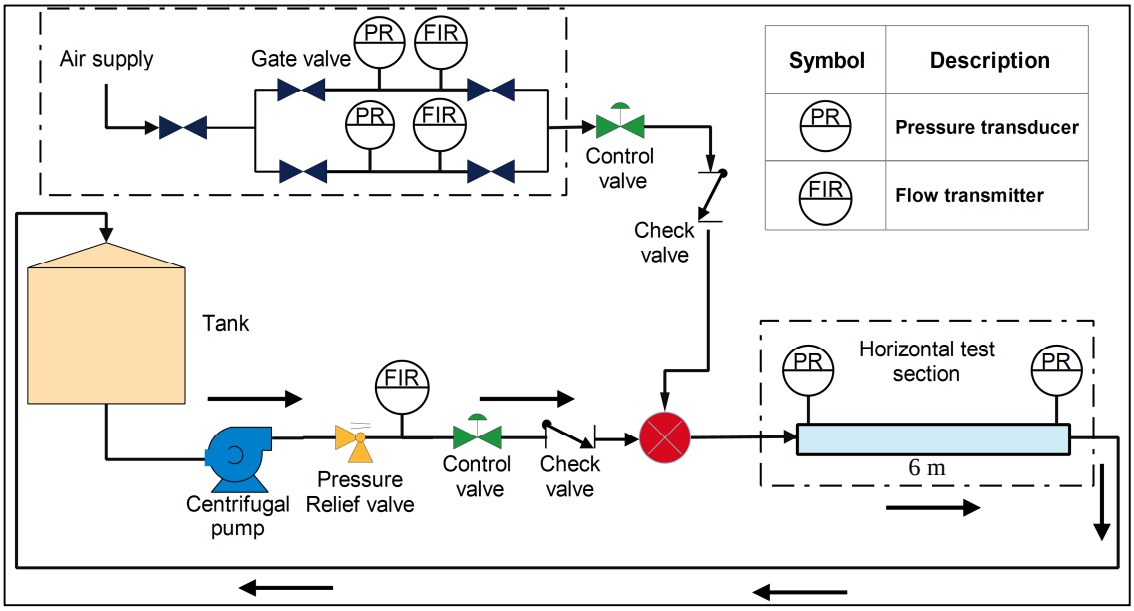

Figure 3.1: Schematic of Experimental Setup (Horizontal Test Section).

3.2 Different Components of the Setup

3.2.1 Pump

The pump used in this setup is desired to circulate a large volume of water at a high-volume flow rate. This has a 5 HP motor, which requires 460 V three phase voltage for operation. The pump has been controlled by TB Wood's inverter, which is shown in Figure 3.2 This inverter can change the frequency of the pump which controls the water flow rate in the flow loop. Moreover, it is also used to turn on/off the pump.

Figure 3.2: TB Wood AC Inverter.

Table 3.1: Pump Specifications.

Brand	Glouds Pump Inlet: DN 100 Outlet: DN 80
Pump Model Number	25SH2J5F0 A0400053
Motor Speed	5 HP, 460V
Water Flow Range	250 lpm – 900 lpm
Pump operation Frequency Range	30 Hz – 65 Hz (Recommended)

3.2.2 **Tank**

This flow loop has a large PVC reservoir tank with a capacity of 1000 L, shown in Figure 3.3. The tank connected to the pump using 101.6 mm diameter pipe.

Figure 3.3: Liquid Reservoir Tank

3.2.3 **Water Flow Meter**

In this flow loop, Omega FTB-730 Turbine Flowmeter (shown in Figure 3.4) has been used to monitor the liquid flow rate. This flowmeter has been mounted before the liquid/gas mixing zone to get the inlet liquid volume flow rate of the gas/liquid two-phase flow. The liquid flowmeter has the capacity to measure around 11 L/min - 1500 L/min liquid flow rate at an accuracy of ±1% (Full Scale).

Figure 3.4: Omega FTB-730 Turbine Flowmeter

3.2.4 **Gas Flowmeter**

There are two turbine air flowmeters used in the inlet air flow line which covers a wide range of air flow rate. In DN15 pipe Omega FLR6725D (2 to 25 SCFM Flowrate) flowmeter and in DN 25 pipe Omega FLR6750D (5 to 50 SCFM) flowmeter have been installed. There are valves in the air flow line which drive the air to the desired flowmeter. Figure 3.5 shows the Omega FLR6750D air flowmeter.

Figure 3.5 Omega FLR6750D air flowmeter.

3.2.5 **Air Flow Line**

The air flow lines consists of components such as air flowmeter, pressure sensors, air check valve, air control valve and air filter. This air flow lines have a DN 15 and DN 25 mild steel pipe which is connected to two different flow meter. DN 15 line has been used to get low air flow rate and DN 25 is to get higher air flow rate. The air enters this flow loop from the central compressor supply which has a shut-in pressure of 680 kPa. There are two pressure sensors (Omega PX603) after the flowmeter to measure the air pressure entering the multiphase flow loop. Moreover, a control valve is placed to control the air input in the multiphase flow loop and a check valve to resist the water from entering in the air line.

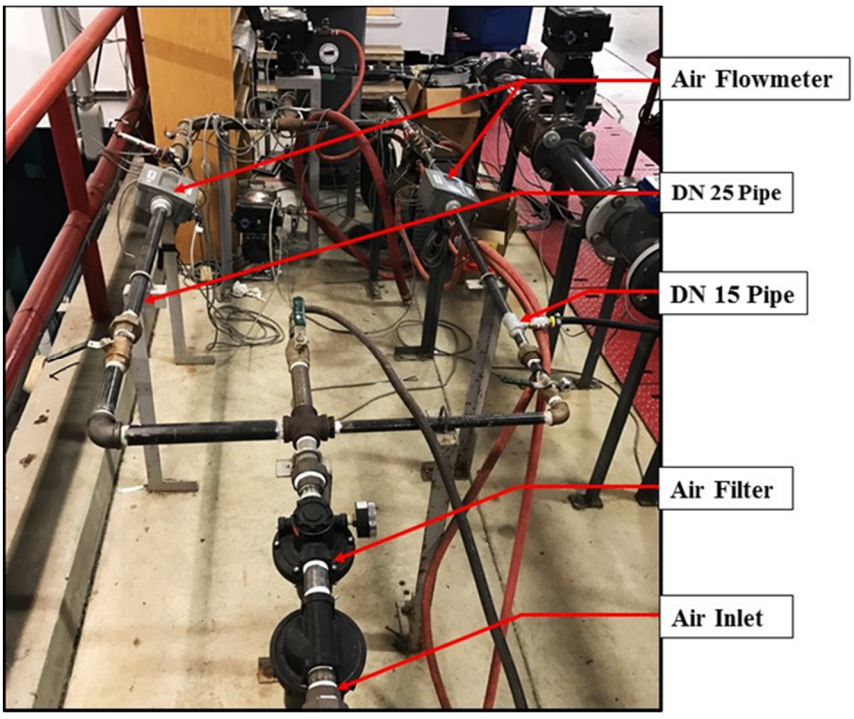

Figure 3.6: Air flow lines

3.2.6 **Pressure Transducer**

There are four pressure transducers used in the flow loop. Two of tem has been installed in the air flow line to measure inlet air pressure and other two of them are in the horizontal test section. Here, Omega PX603-200G5V (0-200psi) has been used in the air lines Omega PX603100G5V (0-100psi) cable type pressure transducer has been used in the horizontal test section. All the pressure sensors have been calibrated using a pressure sensor calibrator set-up, where a known pressure was given in the sensor using an adaptor and then the voltage output was measured for that known input pressure. The obtained voltage values were configured in the Data Acquisition system to get the pressure output. In the Figure 3.7, Omega PX603100G5V has been shown with the calibration curve, where it was attached with the horizontal test section using a clamp fittings.

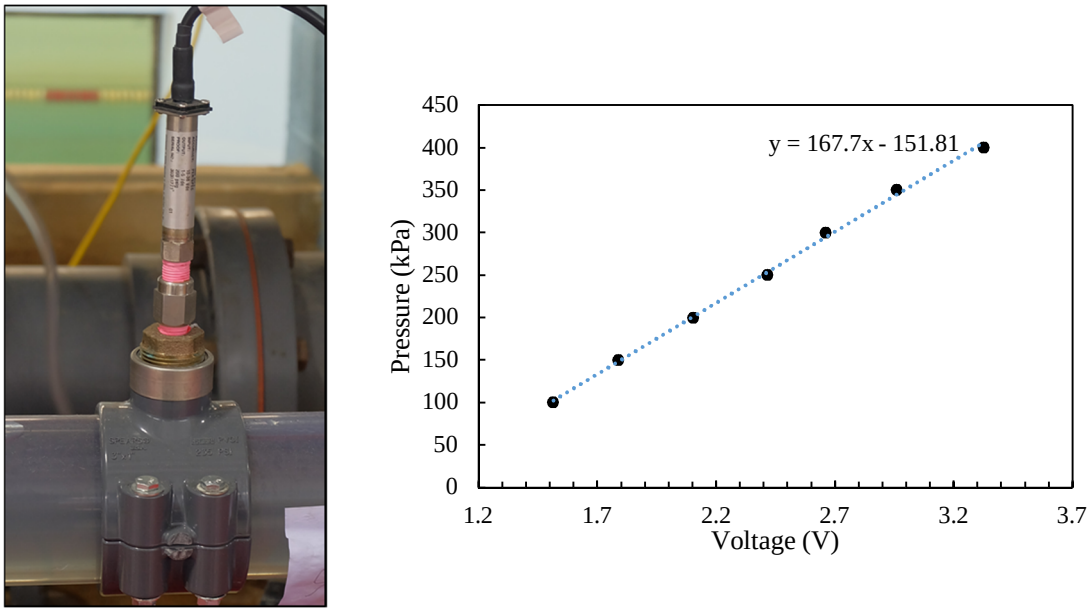

Figure 3.7: Omega PX603100G pressure sensor and the calibration curve.

3.2.7 **Control Valve**

Two VRC VX700 electro-pneumatic positioner and control valve were installed in both water and air line just before gas/liquid mixing zone to control the water and air flow in the flow loop. Here, VRC VX700 electro-pneumatic positioner (shown in Figure 3.8) has not been used with electrical connection and the control valve was used manually to control the flow rates

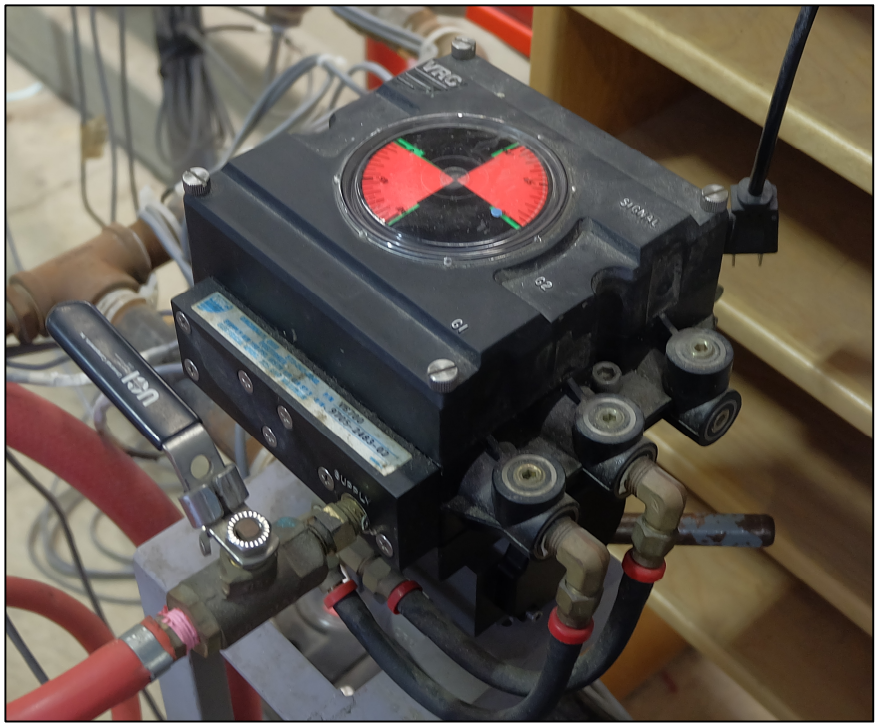

Figure 3.8: Control valve for the air flow.

3.2.8 **Data Acquisition System (DAQ)**

Universal Data Acquisition System from National Instrument, has been used to collect all types of data from flowmeter and sensors. This Data Acquisition System has four NI 9219 universal module with 4 channels each gives 100 sample per second. The modules have been attached with an NI cDAQ-9178 USB chassis. NI Signal Express 2014 has been used as data-logging software for acquiring pressing data from the modules.

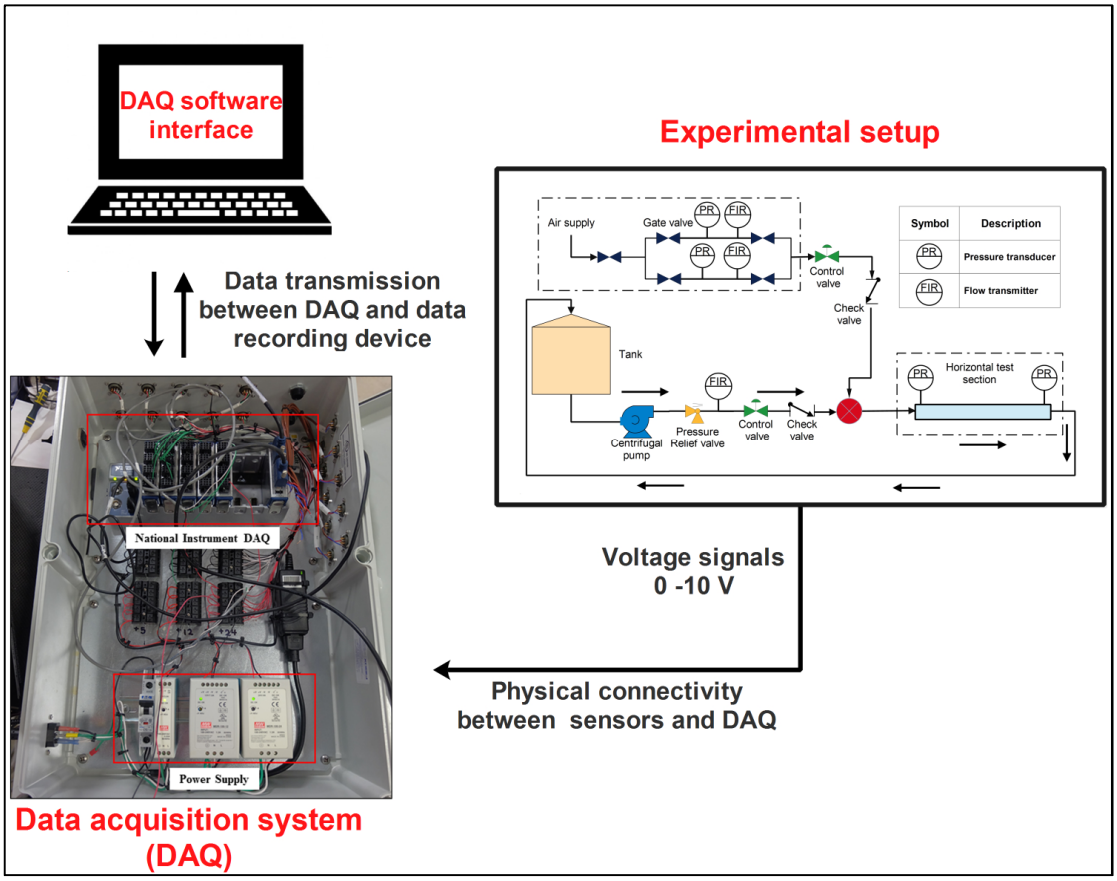

Figure 3.9: National Instrument Data Acquisition System

The Data Acquisition System collected the input signal as voltage (for Pressure Transducer and air flowmeters) and Current (for water flowmeter) through low noise cables and the NI signal express software process that data and give output in kPa and Liter/min units. This software can also record the data for required time and compile it in an excel sheet directly.

3.2.9 **Safety Features**

Pressure Relief Valve

To save the flow loop and the pump from the sudden increase of pressure due to valve or pipe blockage a pressure relief valve has been installed at the inlet section of the water line. It is a DN40 Jaybell pressure relief valve which is shown in the Figure 3.10. It is an industrial standard pressure relief valve consisting of a bypass line.

Figure 3.10: Pressure Relief Valve

Snubber in the Pressure Transducer

Omega pressure snubber (shown in red box Figure 3.11) has been used with each pressure transducer to protect the pressure sensor from water and solid particles. It has a porous metal disc and large filter surface which reduces the risk of sensor orifice clogging.

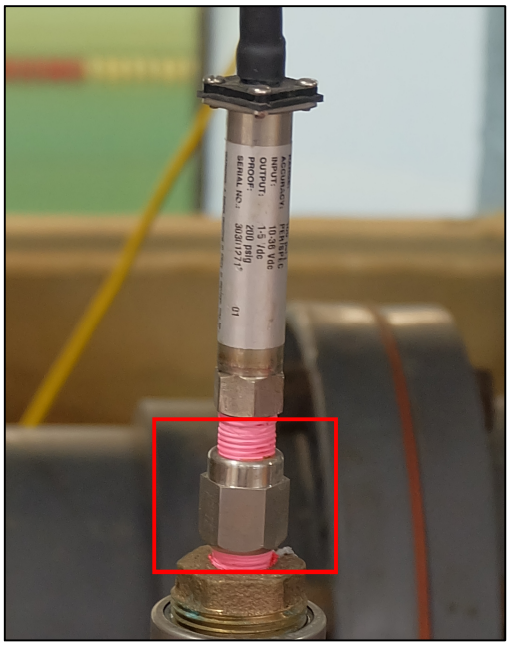

Figure 3.11: Snubber for the pressure transducer.

3.3 Fluid Properties

In two-phase flow experiments gas/Newtonian fluid and gas/non-Newtonian fluid have been used. Here, the Compressed air was used as gas phase, water was used as a Newtonian fluid and 0.1% solution of Xanthan gum was used as the non-Newtonian fluid.

Newtonian Fluid Behavior

Viscosity is one of the important properties of fluid flow, which is the ratio of shear stress to the shear rate, in another word it is the measure of opposing the deformation by shear stress. Whereas, Apparent viscosity is also the ratio of shear stress and shear rate and calculated on shear rate. Apparent viscosity is constant and equal to the fluid viscosity for a Newtonian fluid, but the number changes for non-Newtonian fluid.

For Newtonian fluid, μ is not dependent on shear rate or shear stress, it is dependent on material and its temperature and this viscosity is called Newtonian viscosity. In shear stress versus shear rate graph, the value of μ slope is constant and equal to 1 mPa.s for Newtonian fluid. On the other hand, apparent viscosity is also constant and equal to Newtonian viscosity for Newtonian fluid

Non-Newtonian Fluid Behavior

For non-Newtonian fluid, the apparent viscosity is depended on the liquid shear rate. The shear stress versus shear rate slope become a curved line and does not shows a constant value. It depends on shear rate, flow geometry in the flow path. Typically, non-Newtonian

fluid can be classified into three different types, depending on viscosity. They are shown in Table 3.2 below.

Table 3.2: Types of non-Newtonian Fluid

1. Time Independent Fluid	• Pseudoplastic or Shear-thinning fluid • Viscoplastic fluid • Dilatant or Shear-thickening fluid
2. Time Dependent Fluid	• Thixotropy • Rheopexy or Negative thixotropy
3. Viscoelastic Fluid	

In this study, time-independent fluid, shear thinning or pseudoplastic fluid has been used. Shear-thinning fluid is described by apparent viscosity which decreases with the increase of shear rate. But at a very high shear rate, shear thinning polymer shows Newtonian behavior and shear stress versus shear rate slope curve almost develop into a collinear line (Chhabra & Richardson 1999).

There are many mathematical models developed to determine the non-Newtonian fluid apparent viscosity. Among them the power-law model or Ostwald de Waele model is most commonly used for a limited range. Here the apparent viscosity is shown in the Equation (3.1).

$$\mu_n = \frac{\tau_{yx}}{\gamma_{\dot{y}x}} = m\left(\gamma_{\dot{y}x}\right)^{n-1} \tag{3.1}$$

For, $n<1$, the fluid represents shear-thinning characteristics

$n=1$, the fluid represents Newtonian characteristics

$n>1$, the fluid represents shear-thickening characteristics

In the Equation (3.1), *m* and *n* represent fluid consistency coefficient and flow behavior index respectively or power law index. When *n*=1, it means that the fluid is Newtonian and when *n* value decreases the degree of shear-thinning increases.

Properties of Xanthan Gum Solution

Xanthan gum is the most commonly used industrial biopolymers. Xanthan gum can thicken and stabilize the aqueous system. Xanthan gum solution has significant pseudoplastic properties. Due to these properties, it has a major application the petroleum industries (Gallino et al. 2001). In oil industries, Xanthan gum is widely used in the drilling fluid. It is also broadly used in food industry, cosmetics and pharmacological products.

Xanthan gum is an exocellular heteropolysaccharide formed by a discrete fermentation process. Naturally, a bacterium named Xanthomonas campestris releases this gum. The commercial Xanthan gum also has the same composition and the gum is produced by aerobic submerged fermentation which contains a carbohydrate, a nitrogen source, trace elements and other growth factor (Kobzeff et al. 2003).

Xanthan gum solution has highly pseudoplastic properties. It has shear thinning properties which means, with the rise of shear rate the viscosity of Xanthan gum decreases. But at a

very large shear rate this shear thinning like other polymer solution, Xanthan gum also showed some Newtonian behavior (Chhabra & Richardson, 1999).

A biopolymer company CP Kelco has a Xanthan gum book where different properties of Xanthan gum have been discussed. In that book, some experimental data for various concentration of Xanthan gum at the different shear rate is also shown. The viscosity versus shear rate graph shown in the book is given below in the Figure 3.12.

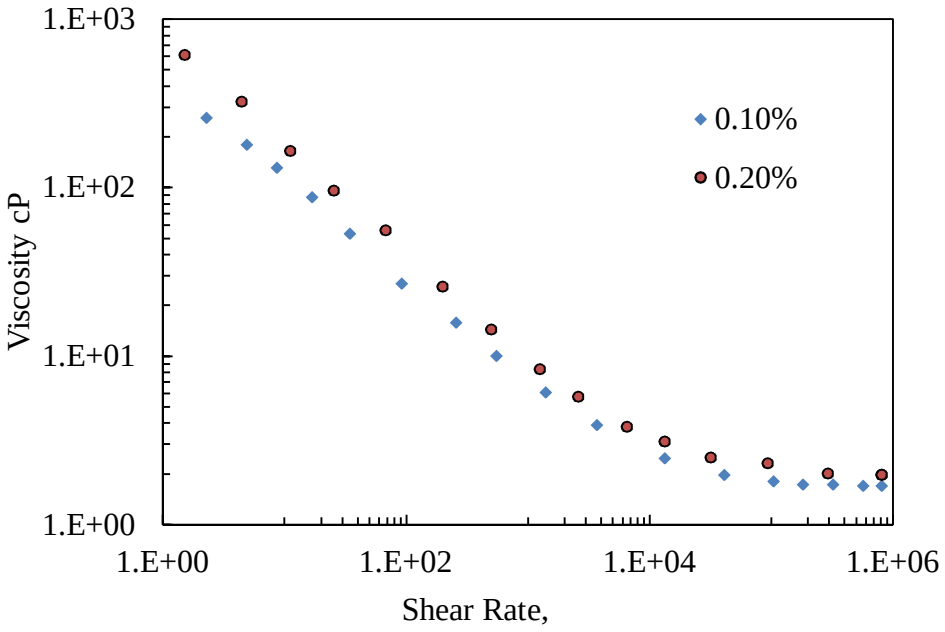

Figure 3.12: Viscosity vs shear rate curve for 0.1% Xanthan gum solution(adapted from CP Kelco Xanthan gum book, page-5).

Viscosity Measurement of Xanthan Gum

In order to analyze the viscosity of 0.1% Xanthan gum solution, CAS 1138-66-2 Xanthan gum from Kelzan XCD Polymer has been used, which is an industrially used dispersible biopolymer for drilling fluid rheology control. To make the 0.1% Xanthan gum solution 1g Xanthan gum powder has been dissolved in 1 Liter of water. Rotational viscometer (Model 800) with 8 rotational speed has been used to measure viscosity.

Another viscometer, Viscolite VL 700 from Hydramotion has been used to measure the viscosity instantly by taking out some sample of 0.1% Xanthan gum solution from the tank. This viscometer (shown in Figure 3.13) is a resonant or vibrational viscometer. The sensor has a shaft with an end mass which vibrates at its natural frequency and loose energy when shear through the fluid and this energy loss is measured to find the viscosity. This viscometer has been a very efficient option to measure the viscosity instantly while doing the experiment.

Figure 3.13: Viscolite VL 700 viscometer.

Experimental Properties of Xanthan Gum Solution

To study the properties of 0.1% Xanthan gum solution, 800 rotational viscometer has been used. To determine the viscosity of 0.1% Xanthan gum solution while doing the experiments in the flow loop, viscolite VL 700 viscometer has been used to determine the instantaneous viscosity of the solution.

The model 800 rotational viscometer has up to 600 rpm and the viscosity versus shear rate curve achieved from this experiment is exhibited in the Figure 3.14. This curve for both 0.1% and 0.2% Xanthan gum shows a similar pattern as the experimental graph prepared by CP Kelco company which is shown in the Figure 3.12. In this experiment, 0.1% Xanthan gum solution has been used. Therefore, shear stress versus shear rate curve for 0.1% Xanthan gum solution is also represented in Figure 3.15. At the low shear rate the graph is showing nonlinear relationship. However, at high shear rate the relationship tends to be linear.

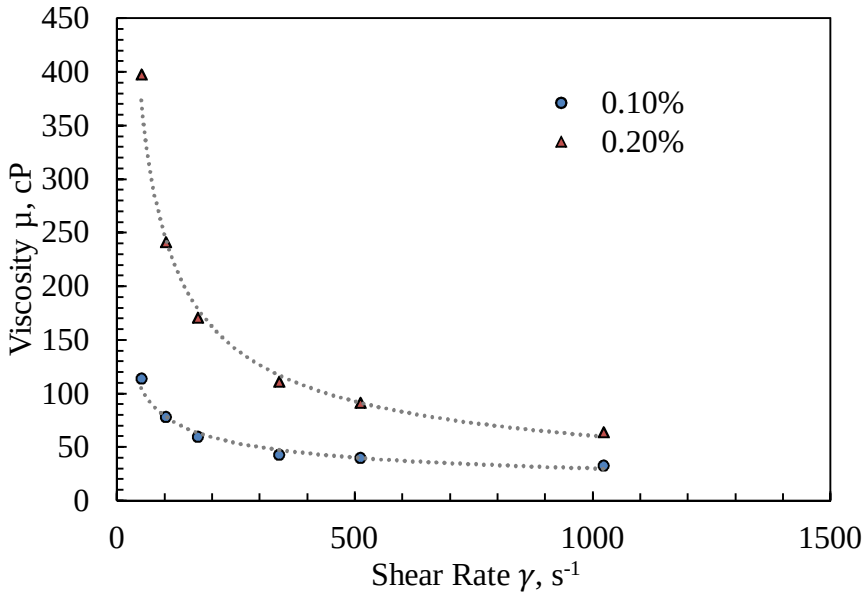

Figure 3.14: Viscosity versus shear rate curve for 0.1% and 0.2% Xanthan gum from the experimental data.

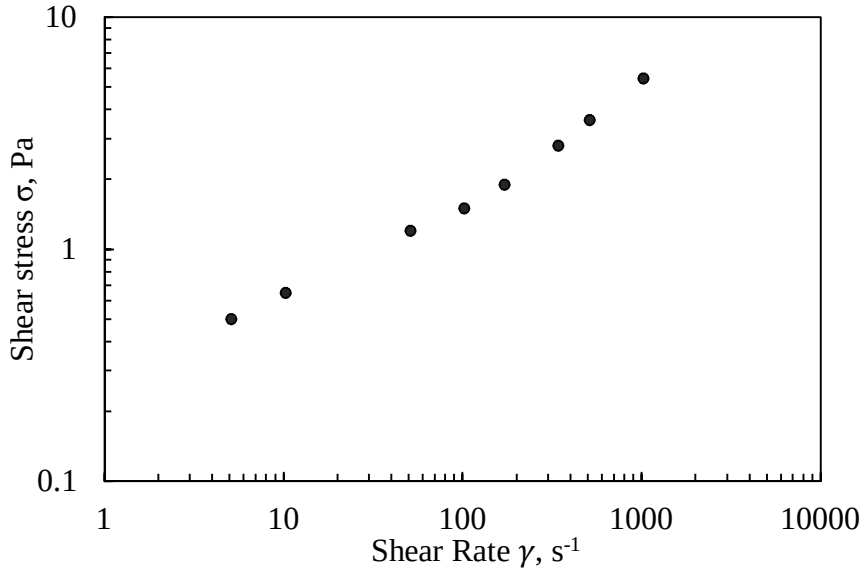

Figure 3.15: Shear stress versus shear rate curve for 0.1% Xantahn gum solution.

In this study, the fluid has been run through the flow loop. The return fluid was discharged in the liquid tank from the top part of the tank, which creates high turbulence inside the tank. Moreover, when the slug flow has been set up in the flow loop, these slugs hit the tank water like bullets which creates more turbulence which tends to create high shear rate. Therefore, this experimental setup mostly gives slug flow, the viscosity change of the 0.1% Xanthan gum solution is not significant in this study.

The model 800 rotational viscometer can only give up to 600 rpm and the apparent viscosity of 5.8 cP. The apparent viscosity is directly related to shear rate and the experimental shear rate is unknown in this study. According to Chhabra & Richardson, (1999) at high shear rate shear thinning fluid shows some Newtonian behavior. While doing the experiments, similar behaviors have been observed with the 0.1% Xanthan gum solution. The fluids of the flow loop was dumped in the tank with high impact and turbulence, also the centrifugal pump gave high shear to the fluid. Thus, one can assume that the shear rate was very high in this setup. When the viscosity was measured in between the experiments, the value also became stable at 2.3 cP to 2.4cP.

After analyzing the data from model 800 rotational viscometer by the shear stress versus shear rate curve and apparent viscosity versus shear rate curve, the following parameters can be determined for 2.4 cP 0.1% Xanthan gum solution which is shown in Table 3.3.

Table 3.3: Specification of 0.1% Xanthan gum

Xanthan Gum Solution	0.1%
Apparent Viscosity at 600 rpm (Using Rotational Viscometer)	5.62 cP
Experimental Viscosity (At higher shear rate and Using Viscolite VL 700 Viscometer)	2.4 cP
Power Law Index, n	0.81
Power Law Index, m (also represent as k)	0.009344

In Table 3.3, $n=0.81$, where n<1. This also exhibits shear-thinning properties of 0.1% Xanthan gum solution, but the value is near the Newtonian fluid's *n* value, which clearly explains the constant viscosity property of the 0.1% Xanthan gum solution through-out the experimental study. Using these parameters different analysis has been done in this study for gas/non-Newtonian fluid which is discussed in the following chapters.

3.4 Conclusion

In this study, the experimental data has been used to obtain an in depth understanding of the two-phase flow phenomena. The two-phase flow analysis became challenging because of the overall length of the flow path. The flow loop is around 20 m long and the liquid and gas flow pipe orientation few times before reaching the test section. This pipe network structure might increase the uncertainty to get required flow characteristics.

Chapter 4. Flow Map

4.1 Introduction

Different forms of flow patterns may be observed when two or more than two phases flow simultaneously. The flow map tries to predict these different types of flow region as a function of superficial liquid velocity plotted in contrast to superficial gas velocity and the boundary line is drawn to separate different flow regime of multiphase flow.

The initial research by Lockhart & Martinelli, (1949) on multiphase flow was done for the horizontal pipe. Later, Baker (1954) performed some experiments for gas/Newtonian fluid flow which brought some notable changes in the Lockhart & Martinelli (1949) equations which could describe flow patterns in horizontal pipelines more effectively. Baker (1954) suggested different correlations for each flow regimes for gas/Newtonian two-phase flow. However, Dukler et al. (1964) performed an experiment with Baker (1954) and Lockhart & Martinelli (1949) pressure drop correlations with an extensive number of data points and concluded that Lockhart & Martinelli (1949) correlation provides a better approximation of flow regimes except in wavy flow. For gas/Newtonian flow there are several flow maps to predict the flow patterns.

Taitel & Dukler (1976) flow map and Mandhane et al. (1975) flow map are the most frequently used flow map for gas/Newtonian flow. These flow maps were drawn for specific condition, as such these flow maps poorly define the flow regime boundary and the transition region for other experimental conditions. Usually, the flow patterns are

visually identified and there is a subjective evaluation of the confined area of the flow regimes which makes the flow maps more ambivalent (Chhabra & Richardson 1999).

Researchers also developed different flow pattern map for gas/non-Newtonian flow. For horizontal gas/non-Newtonian fluid Chhabra & Richardson (1999) developed a flow pattern map by slightly modifying Mandhane et al. (1974) horizontal flow pattern map using the available data of gas/non-Newtonian shear-thinning liquid mixture flow. However, there was not enough data to verify Chhabra & Richardson (1999) flow map for annular and slug flow.

One of the major goal of this study is to comprehend the different type of flow regime for the experiment setup to verify the horizontal two-phase flow map for both gas/Newtonian and gas/non-Newtonian fluid.

4.2 Flow Regimes

In order to estimate the important hydrodynamic features of multiphase flow, it is necessary to have knowledge about the actual flow pattern under definite flow condition. Two-phase flow implies gas and liquid flow through a pipeline system, simultaneously. The gas and liquid interface is deformable, so it's hard to predict the region occupied by gas or liquid phase. When two phases flow through a pipeline, different types of interfacial distribution can form. The variety of flow patterns mostly depends upon their input flux of two phases, size and assembly of the pipe, physical properties of the fluid, etc. There are a huge number of experimental studies on gas/Newtonian or solid/Newtonian fluid flow. But, a limited amount of studies has been done on non-Newtonian multiphase flow.

Usually, two-phase flow implies gas and liquid flow through a pipeline system. Some of the common distribution are: bubbly flow, where there is dispersion of small sized bubbles in liquid; slug flow in which each gas bubbles form a large slug shape that is often a bullet shape; stratified flow, where the liquid and gas phase are disunited and the gas flows on the top as it is lighter than liquid; and annular flow where liquid flow as a film on the pipe inner wall. Different types of flow regime for gas/Newtonian and gas/non-Newtonian flow are discussed below;

4.2.1 **Stratified/Wavy flow**

This flow regime happens for comparably low gas/liquid flow rate where liquid flows at the lower base of the pipe due to gravitational force and the gas-liquid interface is smooth. With the increment of gas flow rate at same liquid flow rate, the gas/liquid interface creates wavy flow. This flow pattern is similar to both gas/Newtonian and gas/non-Newtonian flow. Dziubinski et al. (2004) used highly viscous fluid which had more than 100 mPa.s viscosity.

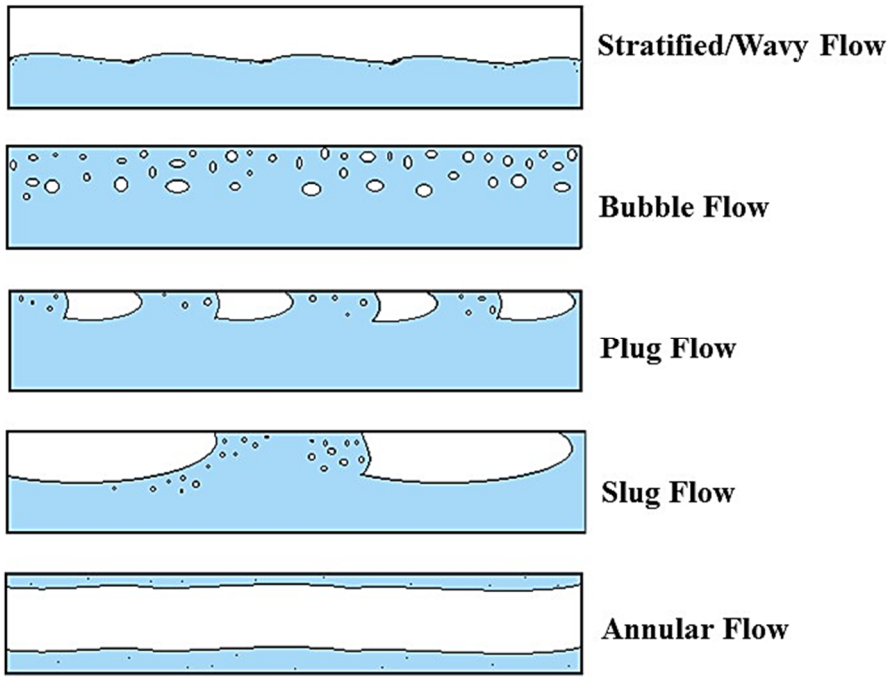

Figure 4.1: Different flow regime for gas/Newtonian flow.

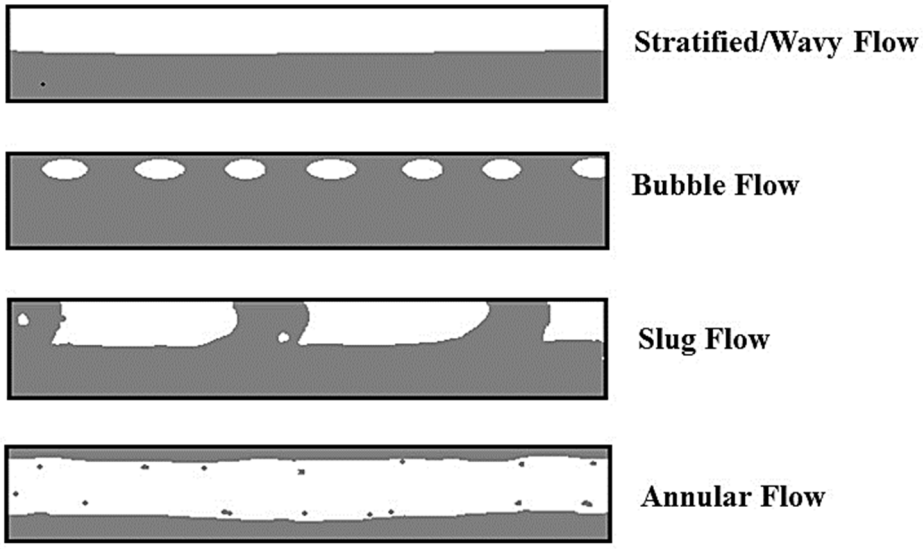

Figure 4.2: Different flow regime for gas/non-Newtonian flow. [Adapted from Dziubinski et al. (2004)]

4.2.2 **Bubble Flow**

This type of flow can occur for a broad range of gas flow rate and high liquid flow rate. In this flow regime, small bubbles are dispersed throughout the liquid and accumulated in the upper portion of the horizontal pipe due to buoyancy. At a low void fraction the gas creates an elongated bubble. Sometimes bubble flow is also referred to as dispersed bubble flow when the liquid flow rate is high. Gas/non-Newtonian flow also show similar bubble flow regime but due to high viscosity the bubbles could not break easily and collide together to form bigger gas bubbles.

4.2.3 **Slug flow**

When the liquid flow rate raised in wavy flow, the waves grow top of the pipe and breaks the continuity of gas flow. This kind of intermittent flow is called slug flow. Plug flow also occurs when the amount of gas increase in bubble flow and the bubble collapse and create small bullet shaped plugs. In other word, when the slug unit is smaller it is called plug flow or elongated bubble flow. In Figure 4.3, the slug unit is divided into two parts; one is slug body or slug region and another is liquid film region. Liquid film region contains liquid film and an elongated gas bubble which is also called Taylor bubble. At higher liquid flow rate, the liquid occupies more space in the liquid film region and the elongated bubble unit become smaller and so with the increase of water flowrate number of slug unit increases. When gas flow rate increases, the elongated bubble become bigger and the liquid film thickness becomes smaller and the number of slug unit decreases with increased gas flow rate.

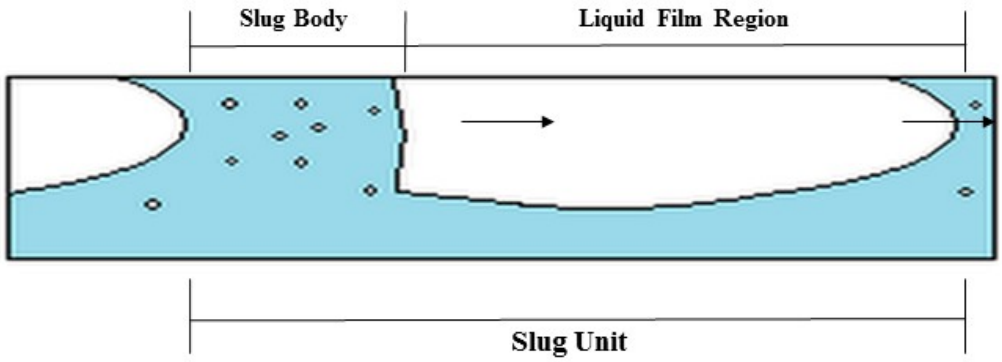

Figure 4.3: Different part of a Slug unit; adapted from Dukler & Hubbard (1975).

4.2.4 **Annular Flow**

Annular flow happens when the gas dwell in the center core of the pipe and the liquid flows along the inside wall of the pipe as a thin layer. When some of the liquid entered in the gas core of the pipe from the liquid film, it is called annular mist flow. This type of flow require high liquid and gas velocity.

4.3 Flow Map for Horizontal Flow

4.3.1 Air/Newtonian Flow Map

The experimental values have been used to verify flow regime map for the horizontal pipe flow. This flow regime map has been compared with that in Taitel & Dukler (1976) and Mandhane et al. (1974) where water and air superficial velocity has been used.

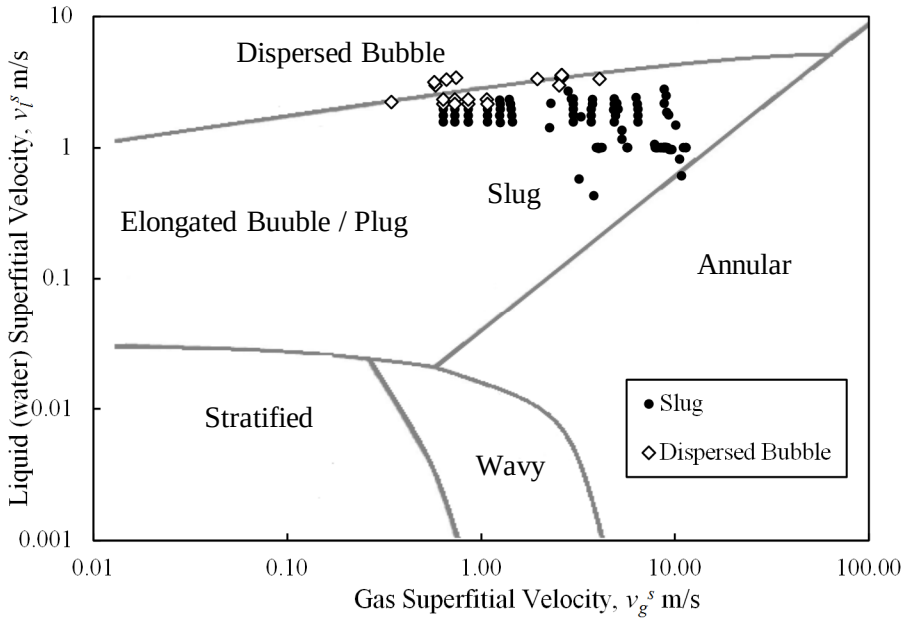

Figure 4.4: Comparison of the Taitel & Dukler (1976) (adapted) flow map with experimental data for horizontal gas/Newtonian flow.

In the Taitel & Dukler (1976) flow map for horizontal pipe (Figure 4.4), most of the experimental data points fall in the respected flow regime area. However, Taitel & Dukler (1976) flow map predicted the dispersed bubble flow better for high gas/water velocity than Mandhane et al. (1974) flow map for this experimental setup.

In the Figure 4.5 below, the Mandhane et al. (1974) flow map has been provided where the data for the slug and dispersed bubble flow data were fitted in the graph accordingly. The map can predict the slug and bubble flow regime. But for high gas and water flow rate, this map cannot predict dispersed bubble flow regime precisely.

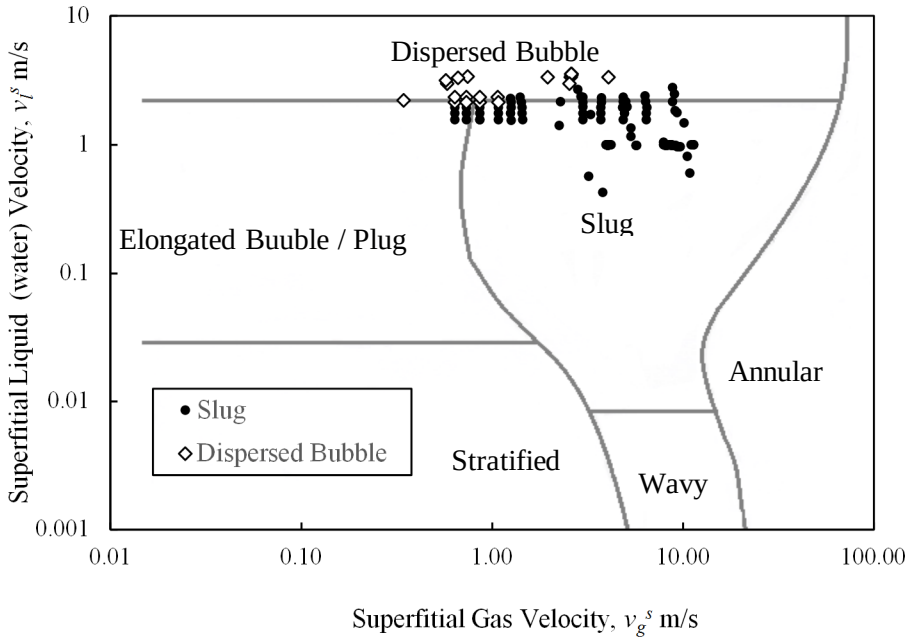

Figure 4.5: Comparison of the Mandhane et al. (1974) (adapted) flow regime map with experimental data obtained for horizontal gas/Newtonian flow.

4.3.2 **Air/non-Newtonian flow map**

Researchers also developed different flow pattern maps for horizontal, vertical and inclined gas/non-Newtonian flow. In Figure 4.6, for horizontal gas/non-Newtonian fluid Chhabra & Richardson (1999) developed a flow pattern map by slightly modifying Mandhane et al. (1974) horizontal flow pattern map. This map has been developed for evaluating the

literature and verified using 3700 data of gas/non-Newtonian shear-thinning liquid mixture flow with 70% certainty. However, there was not enough data to verify Chhabra & Richardson (1999) flow map for annular and slug flow.

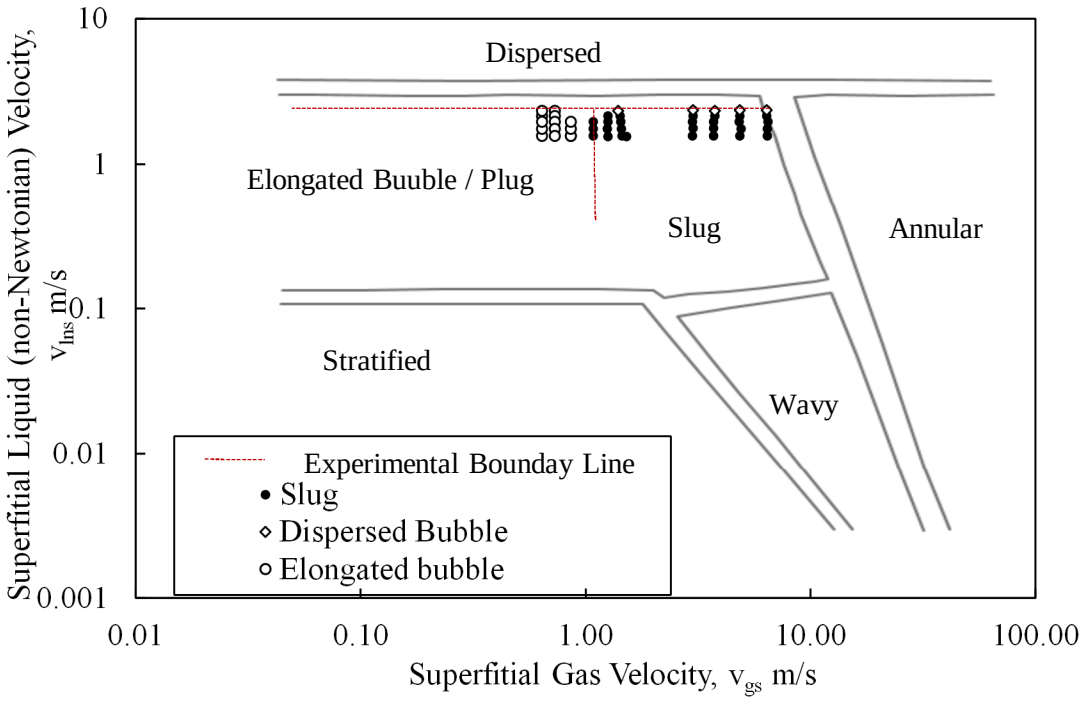

Figure 4.6: Comparison of the (Chhabra & Richardson 1984) (adapted) flow regime map with experimental data obtained for horizontal gas/non-Newtonian flow.

In the above Figure 4.6, the experimental flow regime almost matches with Chhabra & Richardson (1984) flow map, however slug to dispersed bubble flow transition started little earlier for this experiment. Chhabra & Richardson (1984) used particulate suspension of china clay, aqueous polymer solutions, limestone and coal which is much more viscous

shear-thinning non-Newtonian fluid compared to 0.1% solution of Xanthan gum which has been used in this experiment. This is why the dispersed bubble flow regime started earlier.

However, it is beheld that flow patterns of gas/non-Newtonian fluid do not have much difference from gas/Newtonian fluid for horizontal flow. But due to high viscosity, the bubbles and slug could not break easily and collide together to form bigger and well-defined bubbles. However, the transition from one flow regime to another starts at higher liquid and gas superficial velocity combination.

4.4 Conclusions

To conclude it can be said that, these flow maps are reconstructed and validated with the existing literature for identification of the two-phase flow regimes of this experimental setup. The flow loop used in this experiment cannot give stratified, wavy or annular flow and provide a limited bubble flow and plug flow due to the air and water flowrate range. For this reason, other flow regimes could not be verified. Taitel & Dukler (1976) and Mandhane et al. (1974) flow map for air/water two-phase horizontal flow and Chhabra & Richardson (1999) flow map for air/Xanthan gum solution horizontal two-phase flow represented the flow regimes of the experimental setup quite accurately but the transition boundary of the flow regime varied due to the unpredictable characteristics transition zone of the flow pattern

Chapter 5. Slug Frequency

5.1 Introduction

Slug flow is the most usual two-phase flow phenomena experienced in the horizontal or near horizontal pipeline in the practical field. Slug flow in pipeline encountered in different industries like production and transportation of oil and gas, food industry, chemical industry, etc. Slug frequency in other word water hammering leads to various operational problems such as pipeline network instability, equipment damage, pressure fluctuations and vibration of the system. In the oil and gas production industries slug flow also influence the internal corrosion rate increase of carbon steel pipeline. Slug flow creates high turbulence which breaks the pipe wall inhibitor's protection layer (Kouba & Jepson 1990).

Slug flow has bigger bubble flow separated by liquid and combination of these two make the slug unit. Slug Frequency is the number of slug passing a particular point in a specific time in the pipeline. Gas/Newtonian and gas/non-Newtonian flow are the most common flow occurrence in the industries. In the petroleum industries oil-gas flow, drilling fluid flow, slurry flow, gas crude oil flow, etc. are the most frequent gas/non-Newtonian flow phenomena.

To describe multiphase slug flow, slug velocity and slug frequency are the most essential parameters. The most popular and most used slug flow model was described by Hubbard & Dukler (1966) where air-water slug frequency was determined. Gregory & Scott (1969) also used Hubbard & Dukler (1966) slug flow model to determine slug velocity and slug

frequency for their experiment. Rosehart et al. (1975) is the one who studied Non-Newtonian liquid/air two-phase flow slug velocity and slug frequency at the very beginning. An aqueous solution of CMC7H3S, Carbopol 941 and Polyhall 295 was used for liquid phase and the air was used for gas phase in 25.4 mm I.D. horizontal test section. Otten & Fayed (1977) also did Non-Newtonian/air experiment in 25.4 mm I.D. pipe with Carbopol 941-air mixture.

The major objective of this experimental investigation is to understand the slug flow behavior of air/Newtonian and air/non-Newtonian two-phase flow, predicting the slug frequency for different flow condition using both experimental and theoretical models.

In this study, the flow properties and slug frequency of air/water flow and air/non-Newtonian have been analyzed experimentally using one of the unique 60 feet long industrial scale setup with 73.66 mm ID horizontal PVC clear pipe. The experimentally determined slug frequency has been analyzed and the data are compared with the present slug frequency model.

5.2 Slug Velocity

In Hubbard (1965) and Otten & Fayed (1977), experimentally slug velocity was measured by observing a particular slug movement in the test section. They both obtained a relation between slug velocity and no-slip mixture velocity by plotting the experimentally measured slug velocity against no-slip mixture velocity. Hubbard (1965) slug flow model gave better agreement at higher slug velocity. Hubbard (1965) described the relation as,

$$v_s = 1.25\, v_m \tag{5.1}$$

Hubbard (1965) also predicted the true average gas velocity as below. The Equation (5.2) also agreed with other experimental data (Gregory & Scott 1969).

$$v_G = 1.19\, v_m \tag{5.2}$$

It is assumed that Hubbard & Dukler (1966) slug flow model was verified based on one major presupposition that the liquid slug velocity and the maximum gas phase velocity should be similar. Therefore, theoretically, no-slip mixture velocity should be equal to slug velocity.

$$\frac{v_s}{v_m} = C \tag{5.3}$$

Here, C is a constant. Theoretically, C is assumed to be 1.0 for air-water two-phase flow. Hubbard (1965), Rosehart et al. (1975) and Gregory & Scott (1969) considered C value as 1.25, 1.26 and 1.35 respectively for air-water flow. These C values may have varied because of different experimental setup and condition (Otten & Fayed 1977). For non-Newtonian/air two-phase flow Otten & Fayed (1977) compared their results with Rosehart et al. (1975) results where air/Carbopol 941 concentration increased from 0.75% to 0.2%. and C values increased from 1.36 to 1.41, whereas for the same concentration C value of Rosehart et al. (1975) varied from 1.54 to 1.98.

5.3 Slug Frequency

There are different correlations which can predict slug frequency. The first significant model for slug flow was given by Dukler & Hubbard (1975) which predicts different hydrodynamic specification for gas-liquid two-phase horizontal slug flow. Shea et al. (2004) and Hill et al. (1994) predicted slug frequency by considering pipe length whereas, Gregory & Scott (1969), Heywood & Richardson (1978), Gregory and Scott (1969) and Heywood & Richardson (1979) derived simple correlation of slug frequency using fewer variables. Manolis et al. (1995) analyzed slug frequency at high pressure. The most popular model is Taitel & Dukler (1977) model which can be used for extensive range of conditions. These various correlations are discussed below.

In Hubbard (1965) experiment it was found that with the increasing slug velocity the slug frequency decreases. In this experiment, for air-water two-phase flow, we are assuming that slug velocity and mixture velocity are similar. Gregory & Scott (1969) and Hubbard (1965) both showed in their experimental data that there was a minimum value of slug frequency in the slug frequency versus slug velocity (or mixture velocity) graphs for air-water flow. Observing this pattern in the graphs, Gregory & Scott (1969) suggested a velocity dependent empirical equation where slug frequency was correlated with a form of Froude number which is described below.

$$N_{f_s} = \frac{v_l}{gd}\left[\frac{(v_m^0)^2}{v_m} + v_m\right] \tag{5.4}$$

Here, v_m^0 was taken 6 m/s and from slug frequency versus slug Froude number graphs Gregory & Scott (1969) achieved the following equation.

$$f_s = 0.0157\left(N_{f_r}\right)_{slug}^{1.20} \sec^{-1} . \quad (5.5)$$

From the Equation (5.5), Gregory and Scott (1969) described a slug frequency correlation based on his liquid-gas two-phase flow experimental data where water and carbon dioxide is used in 19 mm ID pipe.

$$f_s = 0.0226\left[\frac{v_l^s}{gd}\left(\frac{19.75}{v_m} + v_m\right)\right]^{1.2} \quad (5.6)$$

Here, $v_m \; and \; v_l^s$ are the mixture velocity and superficial liquid velocity of liquid and gas respectively. Therefore, this slug frequency can be combined with Froude number established on superficial liquid velocity.

Greskovich & Shrier (1972) reorganized Gregory & Scott (1969) correlation which is given below.

$$f_s = \left[0.0425\frac{v_l^s}{v_m}\left(\frac{2.02}{d} + \frac{v_m^2}{gd}\right)\right]^{6/5} \quad (5.7)$$

Zabaras & others (1999) described another correlation based on 399 data points with smallest average absolute error and standard deviation for both horizontal and inclined pipe

flow. This correlation is the modification of Gregory & Scott (1969) correlation, and the unit is in English unit which is shown in the Equation (5.8). Where θ is the inclination angle. The experiment was done with air and water.

$$f_s = \left[0.0425 \frac{v_l^s}{gd}\left(\frac{1}{0.0506 v_m} + v_m\right)\right]^{6/5} [0.836 + 2.7\, sin^{0.25}\, \theta] \qquad (5.8)$$

Heywood & Richardson (1979) determined liquid volume fraction for air-water two-phase flow utilizing the gamma-ray technique in 41.91 mm ID horizontal pipe. To determine liquid volume fraction, they used power spectral density function and probability density function. These features are also helpful to determine different slug flow characteristics such as the value of average film and slug volume fraction, average slug frequency, and average slug length. The slug frequency correlation was determined by curve fitting the data and λ is the liquid volume fraction where, $\lambda = v_l^s/(v_l^s + v_g^s)$ and d is the pipe diameter.

$$f_s = \left[0.0462\, \lambda \left(\frac{1}{0.0126 d} + \frac{v_m^2}{gd}\right)\right]^{1.02} \qquad (5.9)$$

Shea et al. (2004) developed a correlation describing slug frequency as a function of pipe length. In the slug frequency Equation (5.10), v_l^S is the superficial liquid velocity, d is the pipe diameter and l_p is the pipe length. This correlation is based or curve fitting of field and laboratory data, not based on theoretical analysis. In this equation, it is also shown that the slug frequency is inversely dependent on the pipe length l_p, which does not agree with

the other theoretical analysis. According to Al-Safran (2009), OLGA 2000 slug tracking model had some time delay problem between two slug, to solve this issue Shea et al. (2004) correlation was initially used. Moreover, the pipe length can be questionable for long distance transmission system with hilly condition.

$$f_s = 0.47\left[\frac{(v_l^s)^{1.5}}{l_p^{1.1}d^{2.4}}\right]^{0.5} \tag{5.10}$$

Picchi et al. (2015) described a slug frequency equation which considers the rheology of the shear-thinning fluid. This equation is the modified version of Gregory & Scott (1969) correlation. In the Equation (5.10), $Re_w = \frac{\rho_w v_l^s d}{\mu_w}$ is the water Reynolds number and $Re_n = \frac{d^n v_{l_n}\rho_n}{m8^{n-1}\left(\frac{1+3n}{4n}\right)^{n-2}}$ is the power-law fluid Reynolds number at superficial condition, where *n* and *m* is the fluid behavior index.

$$f_s = 0.0448\left[\frac{v_{l_n}}{gd}\left(\frac{32.2014}{v_{m_n}} + v_{m_n}\right)\right]^{.88} n^{-2.85}\left(\frac{Re_n}{Re_w}\right)^{.07} \tag{5.11}$$

5.4 Experimental Results

5.4.1 Air/Newtonian Two-phase flow

Table 5.1: Experimental Parameters

Newtonian Fluid	Water
Non-Newtonian Fluid	0.1% Xanthan Gum solution
Liquid Velocity Range	1.5 m/s to 2.5 m/s
Air Velocity	2.8 m/s to 6.4 m/s

The slug frequency data has been discussed in terms of mixture velocity, liquid velocity and Froude number and Reynolds number.

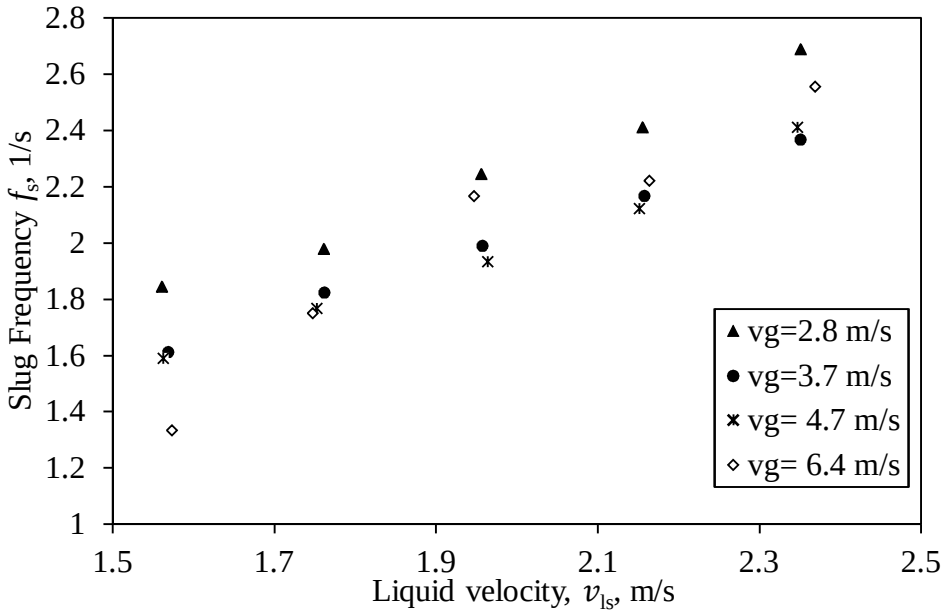

Figure 5.1: Effect of liquid superficial velocity on slug frequency for air/water flow.

Figure 5.1 shows that slug frequency increases with the increase of liquid superficial velocity for all test combination while the superficial gas velocity was kept constant for each set of data. This happened due to the increase in liquid volume fraction. The liquid occupies more space in the liquid film region as the elongated bubble unit become smaller which is why slug unit increases in number. In Figure 5.2 effect of superficial gas ratio on slug frequency has been shown. For a constant liquid flow rate slug frequency decreased with increasing gas velocity created an inverted curve. The slug frequency decreases when the gas velocity increases until around 5 m/s gas flow rates and then starts increasing.

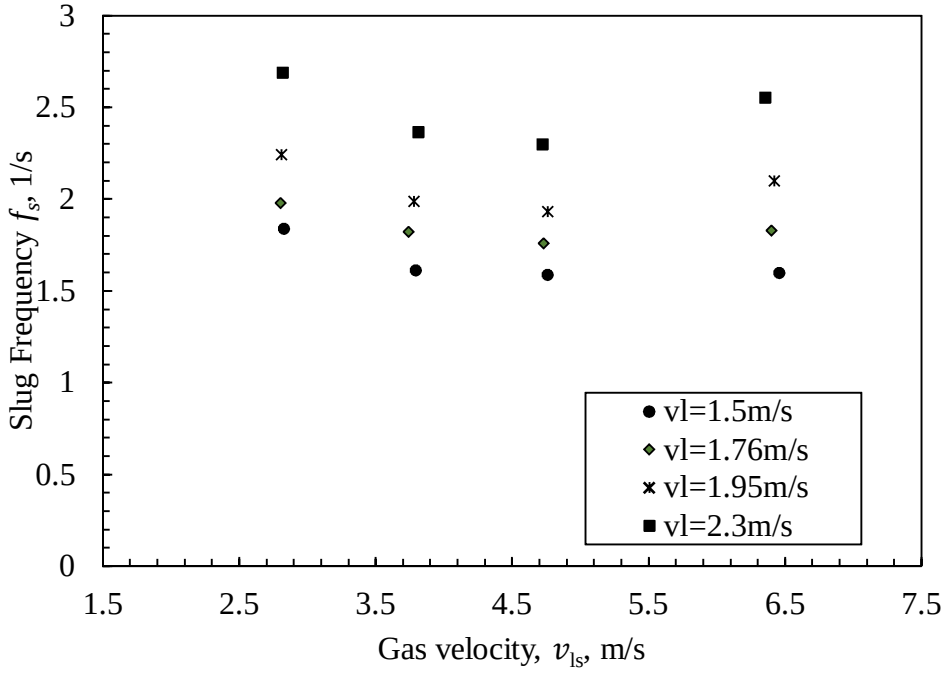

Figure 5.2: Effect of gas superficial velocity with slug frequency for air/water two-phase flow.

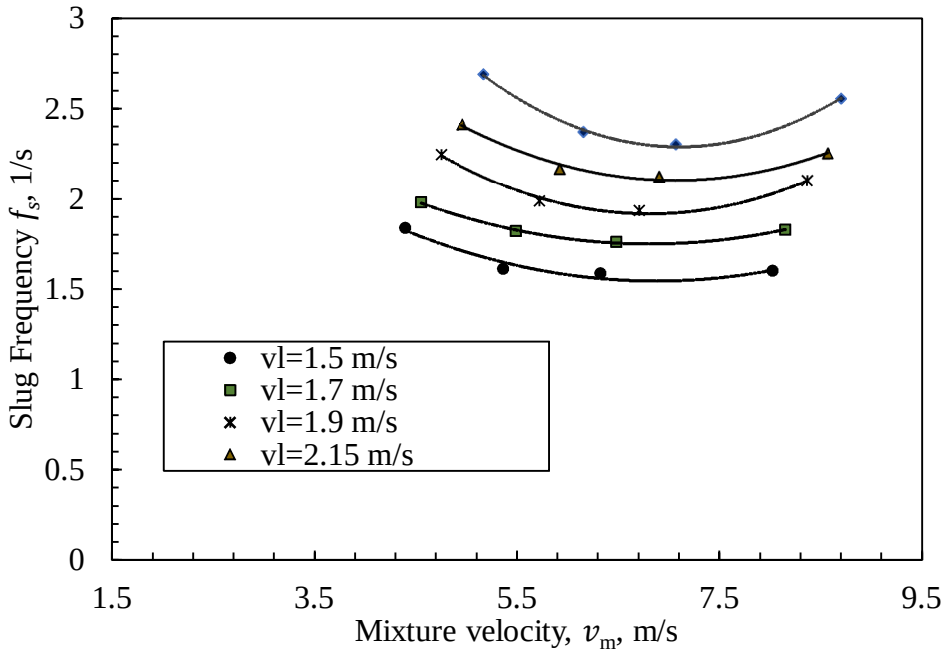

Figure 5.3: Slug frequency vs mixture velocity for air/water flow.

Comparing Figure 5.2 and Figure 5.3, the slug frequency curves mainly depends on superficial gas velocity. Two of these graphs also show that at 5 m/s to 6.5 m/s the slug frequency became minimum and the slug frequency increases with increasing mixture velocity or gas superficial velocity. This phenomenon occurred due to the transition from slug to dispersed bubble flow. At higher gas flow rates, the turbulence in the flow starts increasing and the slug units start to break down and the number of slugs increases. It has also been observed that amount of dispersed bubble increases in the slug pocket and liquid film area. This indicates the starting of transition of the flow pattern. Moreover, these graphs totally agree with Otten & Fayed (1977) and Gregory & Scott (1969) experimental data.

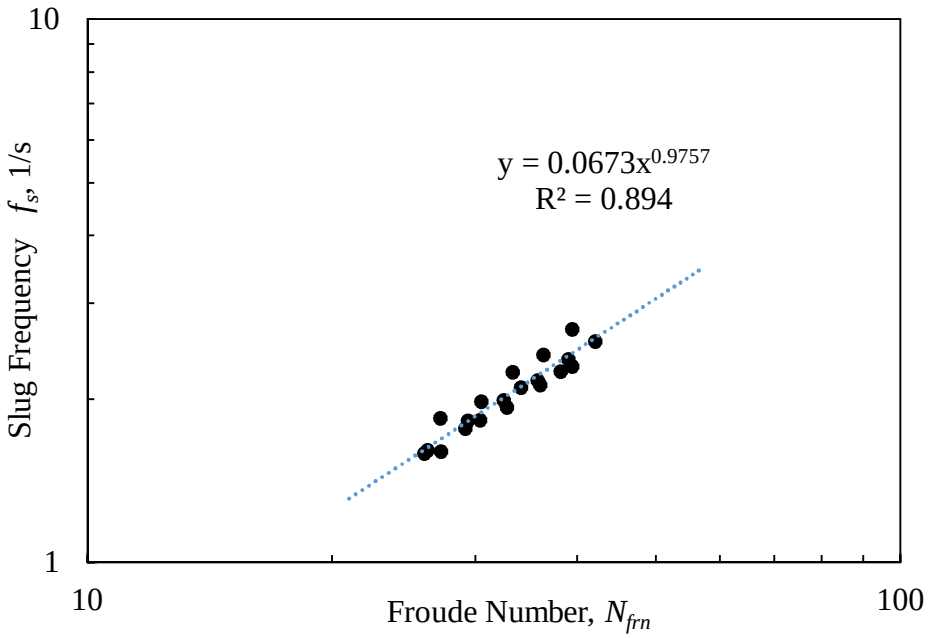

Figure 5.4: Slug frequency versus Froude number for air/water flow.

In Figure 5.4, the slope of slug frequency versus slug Froude number gave an equation where $f_s = 0.0673 \left(N_{f_r} \right)^{0.098}$. This equation shows a deviation from the Gregory & Scott (1969) which is shown in the Equation (5.5), because of the experimental conditions and the assumption $(v_m = v_s)$ for air-water flow of this experiment.

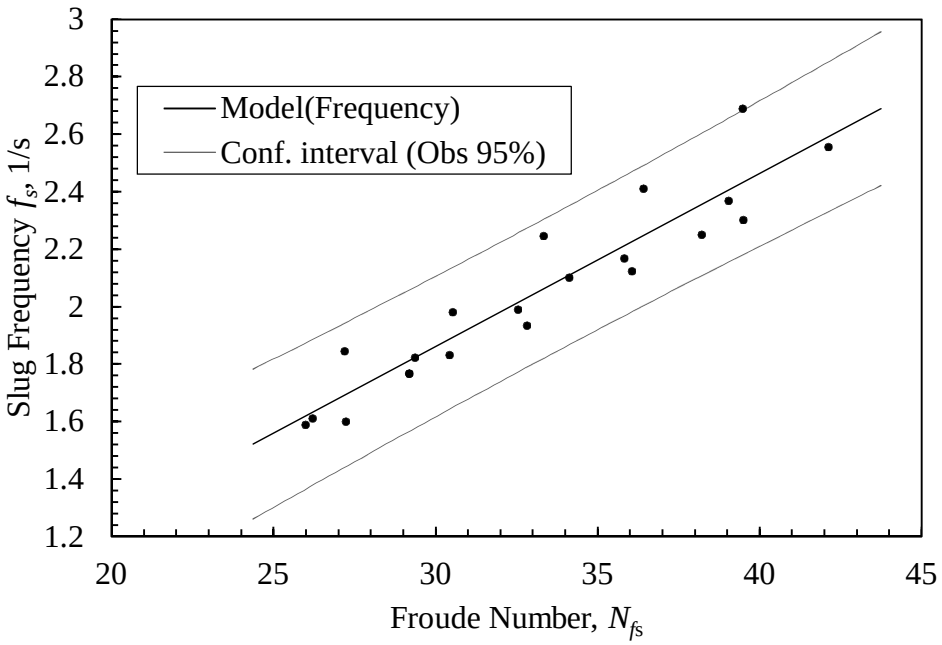

Figure 5.5: Regression of Slug frequency by Froude number graph and the strength of the model R^2=88.1%.

In the above Figure 5.5, the goodness of fit R^2 value is 88.1%. Which means the slug frequency versus Froude number data are close to the regression line and this equation $f_s = 0.0673 \left(N_{f_r} \right)^{0.098}$ can explain the variability of the data around its mean.

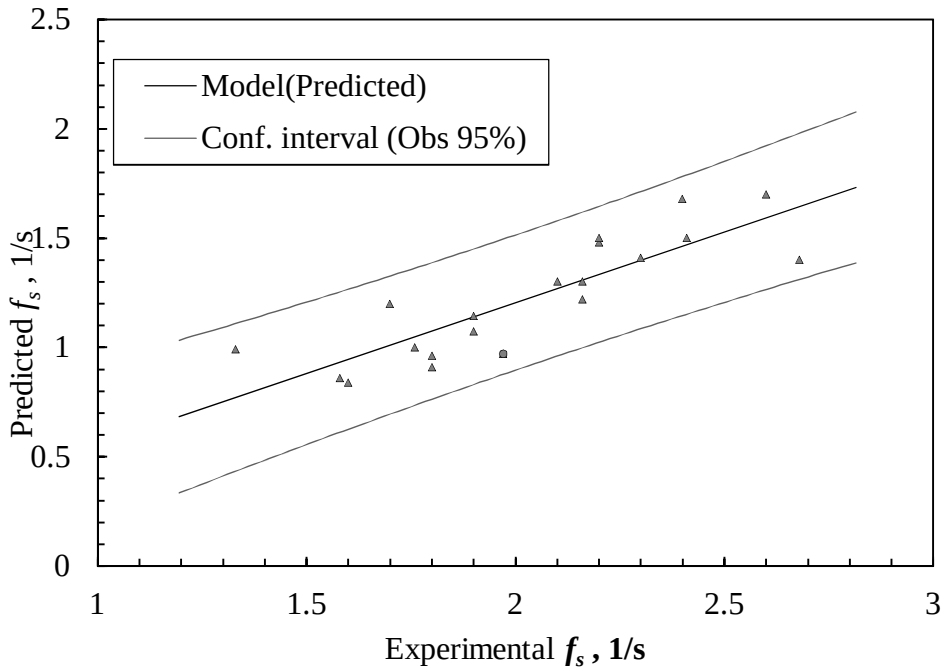

Figure 5.6: Experimental slug frequency for air-water system compared with the predictions model of Gregory & Scott (1969) correlation. [R^2=73.8%]

In Figure 5.6, the experimental data has been compared with the Gregory & Scott (1969) slug frequency model and it is observed that all the data point are close to the regression line and has an R^2 value of 73.8% and all the experimental data fitted well in the 95% confidence interval.

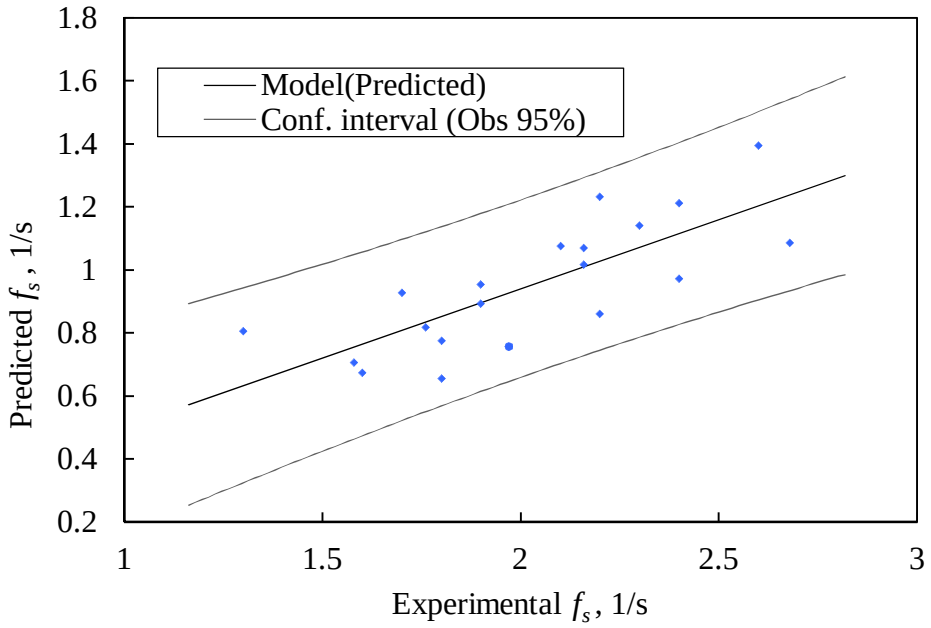

Figure 5.7: Experimental slug frequency for air-water system compared with the predictions model of Zabaras et al. (2000) correlation. [R^2=60%]

The experimental data and the predictions of slug frequency by Gregory & Scott (1969) has an R2 value of 73.8% and Zabaras et al. (2000) have an R2 value of 60%. Therefore, Gregory & Scott (1969) model is close to the experimental data. In the above graph difference between experimental and predicted slug frequency values varied because of the difference in experimental conditions and setup, such as pipe diameter, length, velocity range, etc. (Abed & Ghoben 2015). Also, Figure 5.8 represents 95% confidence interval of the data and none of the confidence interval includes zero which means the data are statistically significant and repeatable data for air/water two-phase flow. Overall, the

experimental data has approximately 5% standard deviation for three samples at the same experimental condition.

5.4.2 **Air/non-Newtonian Two-phase flow**

In this air/non-Newtonian fluid experiment, 0.1% solution of Xanthan gum has been used as air/non-Newtonian fluid.

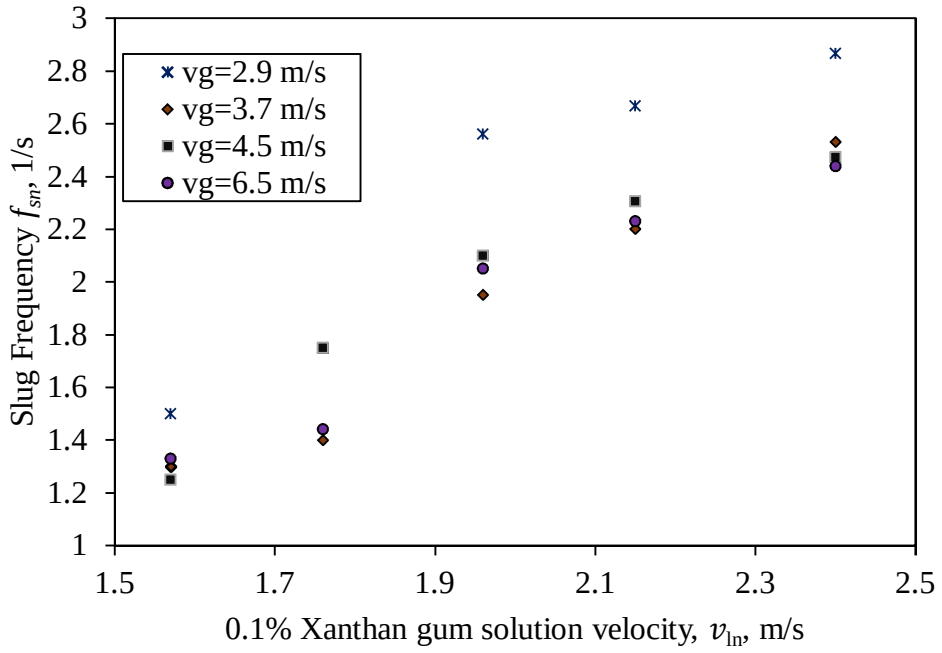

Figure 5.8: Effect of liquid superficial velocity with slug frequency for air/non-Newtonian flow.

In the above Figure 5.8, the slug frequency increases with the increment of liquid non-Newtonian superficial velocity when superficial gas velocity is kept constant. Therefore, at lower superficial liquid velocity the slug frequency increases sharply and at higher liquid

velocity slug frequency decreases. As the liquid velocity increases the air required more energy and air to drive the viscous fluid but the air flow rate is constant for each set. That is why the number of slug decreases as the liquid velocity increases at constant air flowrate.

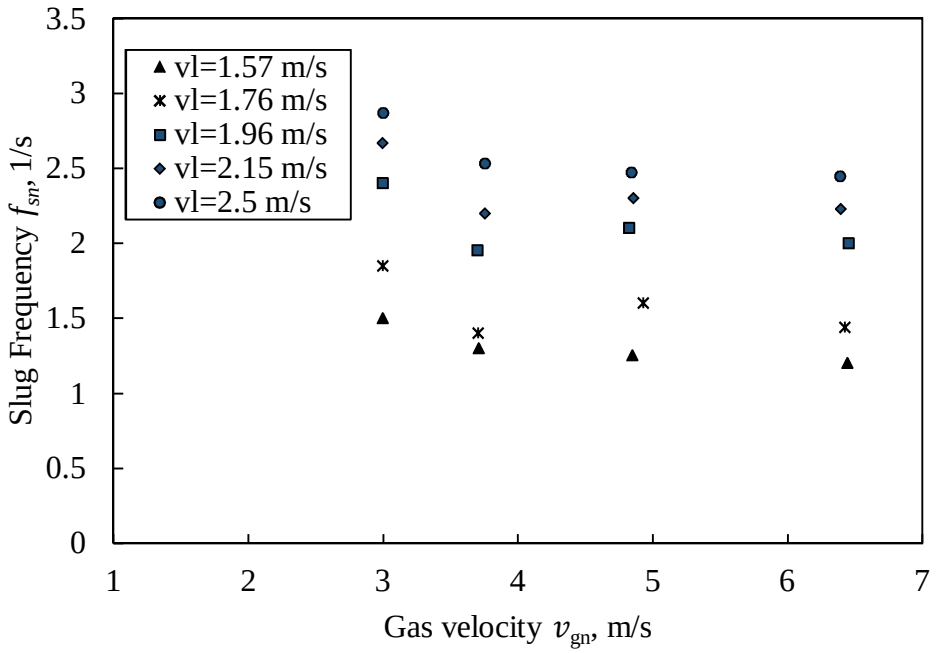

Figure 5.9: Effect of gas superficial velocity with slug frequency for air/non-Newtonian flow.

In the Figure 5.9, slug frequency change has been shown with superficial gas velocity for a constant liquid superficial velocity. Here, 0.1% Xanthan gum solution has been used as non-Newtonian fluid where power law index n=0.81 and k=0.009344. From the Figure 5.9, the slug frequency decreases as the gas velocity rises until 6 m/s. Because, as

the gas flow rates increase in a constant liquid velocity the Taylor bubbles become bigger, therefore, the length of the slug unit increases and slug frequency decreases.

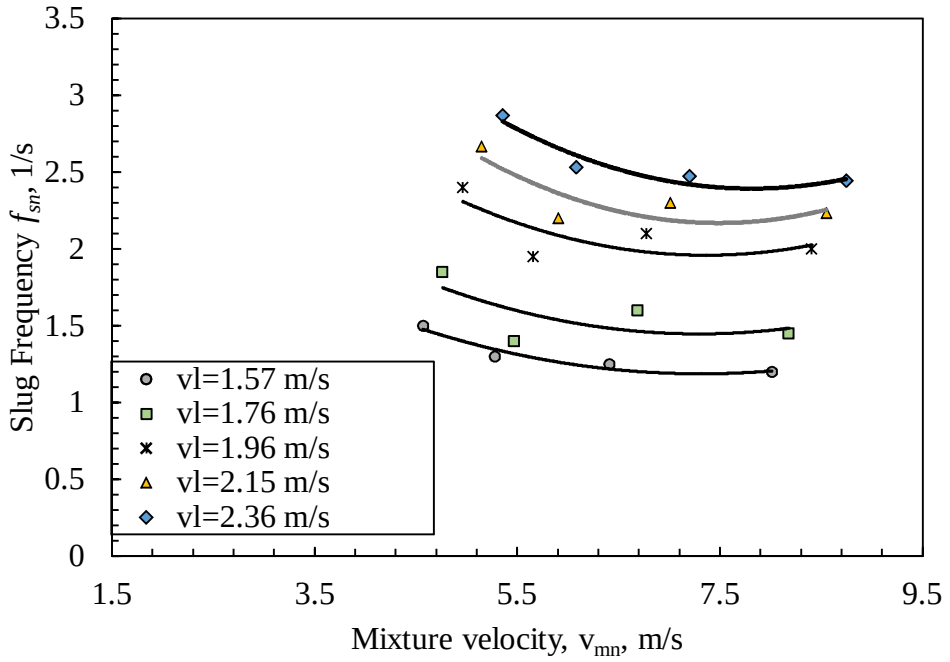

Figure 5.10: Slug frequency vs mixture velocity for air/non-Newtonian fluid flow.

Figure 5.10, represents the change of slug frequency with the mixture velocity of air-Xanthan gum flow. It is also seen that till 6.5 m/s mixture velocity, slug frequency is minimal. Otten & Fayed (1977) also got the similar patterns for his air/non-Newtonian flow. Similar phenomena also occurred in Figure 5.3 for gas/Newtonian flow. But the minimum slug frequency was around 5 m/s mixture velocity which occurred a lot earlier than the gas/non-Newtonian two-phase flow. Here, we can observe a certain effect of

viscosity. Water viscosity at 20℃ room temperature is around 1 cP and the experimental viscosity of 0.1% Xanthan gum is 2.4 cP, which is little more viscous than the water.

The flow mechanism of slug flow is that the gas bubble is trapped in between water and drives water forward almost at the same velocity as gas velocity. But when the liquid become viscous the gas required more energy to drive the liquid forward. At a constant air flow rate, it is hard to achieve extra energy, so the whole process becomes slow and the slug velocity and a number of slug decrease (Rosehart et al. 1975). If further experiments have been done for gas/non-Newtonian fluid, there is a possibility of slug frequency increasing again with increased gas flow rate in the slug to bubbly flow transition zone as the gas/water two phase flow. Where the turbulence of the flow structure starts increasing and the unit slug starts to break down and number of slug increases at higher gas flow rates. It has also been observed that amount of dispersed bubbles increase in the slug pocket and liquid film area. This indicates the starting of transition of the flow pattern.

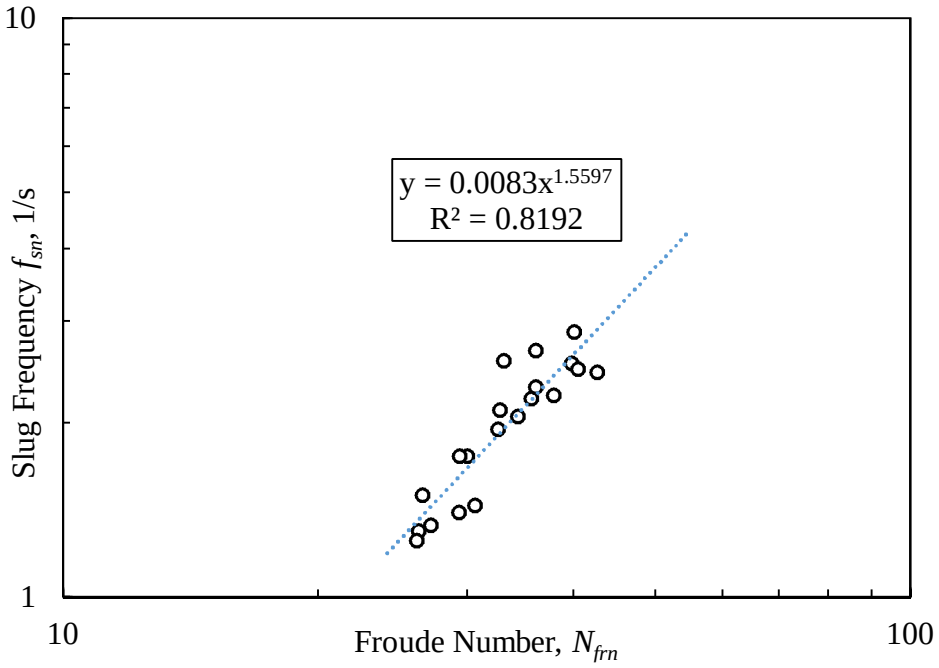

Figure 5.11: Slug frequency versus Froude number for Air/Xanthan gum solution.

As shown in the above Figure 5.11, above it has been shown that the slope of slug frequency versus slug Froude number for air/Xanthan gum solution can be modeled using the equation, $f_{sn} = 0.0083 \left(N_{f_r} \right)^{1.5597}$, where the model strength R^2 is 81.92%.

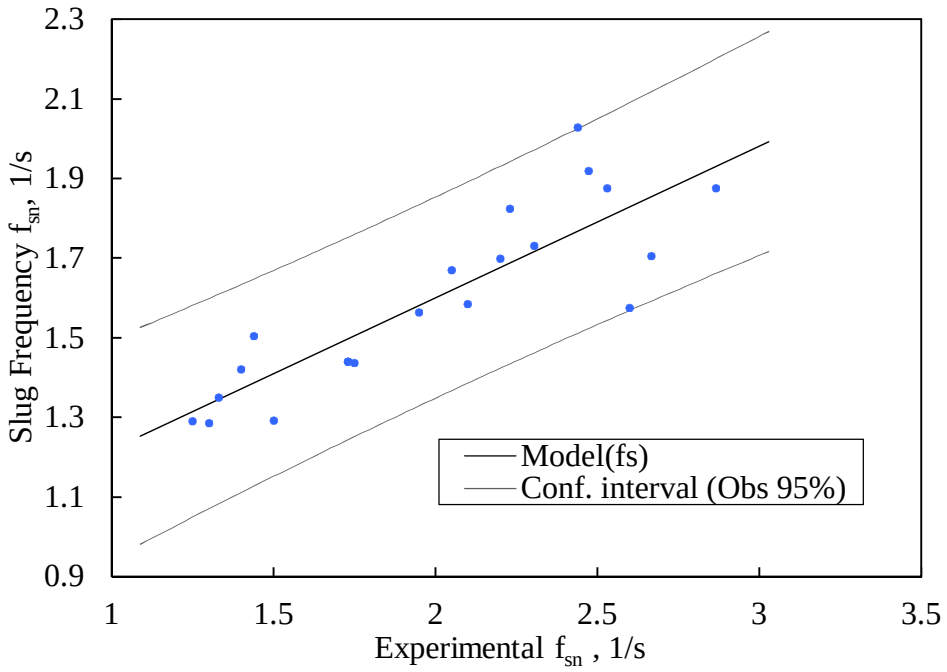

Figure 5.12: Experimental slug frequency for air-Xanthan gum system compared to the predictions by Gregory & Scott (1969) correlation where R^2=74.6%

Picchi et al. (2015) modified the slug frequency equation of Gregory & Scott (1969) for the shear thinning non-Newtonian fluid. Figure 5.12 represents the comparison of experimental result with the modified Gregory & Scott (1969) slug frequency equation. The R^2 value of 75.3% also represents the reliability and repeatability of the experimental data of this study. Also, the experimental data has 95% confidence interval.

5.5 Conclusion

To conclude, the slug frequency analysis shows gas/Newtonian and gas/non-Newtonian fluid have a significant difference in slug properties. The viscosity effect creates the major difference between gas/Newtonian and gas/non-Newtonian fluid. As non-Newtonian fluid 0.1%, Xanthan gum has been used to get fluid of 2.4 cP viscosity. This viscosity is quite close to water viscosity 1 cP. The air/water slug frequency decreased till approximately 5 m/s air velocity and again increased with the increased air velocity. However, the air/Xanthan gum solution did not show similar effect rather the slug frequency slowly decreased with the increased air velocity within the experimental data range. This is the viscosity effect which delayed the transition process.

Chapter 6. Signal Analysis

6.1 Introduction

In multiphase flow phenomena, different forms of flow patterns may be observed when two or more than two phases flow simultaneously. When two or more types of liquid, gas or solid phases flow together the interaction between the phase create different flow patterns. Bubble flow, plug flow, slug flow and annular flow are the basic follow pattern for the horizontal flow. To identify the flow patterns, primarily experimental inspection has been the most common methods. The other methods are, high-speed photography, volume fraction fluctuation, gamma ray tomography, particle image velocimetry (PIV), neutron radiography, pressure fluctuation, etc. Among these pressure fluctuation analysis has been one of the common and simplest methods but due to its nonlinear and unsteady behavior analyzing the data is a challenge (Ding et al. 2007).

Tutu (1982) and Drahos et al. (1987) characterized two-phase horizontal flow regime pressure fluctuation. Drahos et al. (1987) used probability density function (PDF) where a strain gauge pressure transducer was used in 50 mm I.D. Perspex pipe. Sun et al. (2013) used norm entropy wavelet decomposition to analyze gas/liquid two-phase flow pressure signal data across a bluff body. Here, inner pipe diameter was 50 mm and piezoresistive differential pressure sensor and the pressure signals have been analyzed using four levels and four scales Daubechies wavelet (db4) which provided sixteen wavelet packet coefficients. This study also suggested some entropy based two-phase flow map with an identification rate of 95%. Blaney (2008) used gamma ray to identify flow regimes and

continuous wavelet transforms to analyze gamma count data. Park & Kim, (2003) have done wavelet packet transform to analyze pressure fluctuations in a bubble vertical column. Furthermore, De Fang et al. (2012) also used wavelet analysis to understand the gravity differential pressure fluctuation signal perpendicular to the horizontal flow of different flow pattern and the flow pattern transition of gas/liquid two-phase flow in the horizontal pipe. Here, Haar wavelet with six level has been used to decompose the pressure signal and then the energy value has been obtained for each scale. For identifying two-phase flow regime Elperin and Klochko (2002) also used eight-level db4 wavelet transformation to process time series of measured differential pressure fluctuation.

In this study pressure transducer signal data of different flow pattern has been analyzed using wavelet transform to find the pressure signal characteristics of various flow regimes. Wavelet analysis can be used to get low frequency or high-frequency information as it gives the opportunity to use long time interval or short region of a signal. On the other hand, Fourier analysis split a signal into a sinusoidal component of distinctive frequencies. While transforming the signal into frequency domain the time information gets disappeared and it is not possible to understand when an event occurred in the signal. To reduce this drawback Gabor (1946) used Short-Time Fourier Transformation (SFT) where a small portion of the signal is used at a time but the problem is the size of the window cannot be changed once it is selected. Wavelet analysis overcomes all these deficiencies and use time-scale region instead of time-frequency region (Misiti et al. 1996).

6.2 Wavelet Analysis

Wavelet analysis is one of the effective ways of signal processing. Wavelets are asymmetrical and uneven waveforms of adequately limited duration which have a zero average value. Wavelet analysis breaks up the mother wavelet signal into shifted and scaled version which is shown in the Figure 6.1.

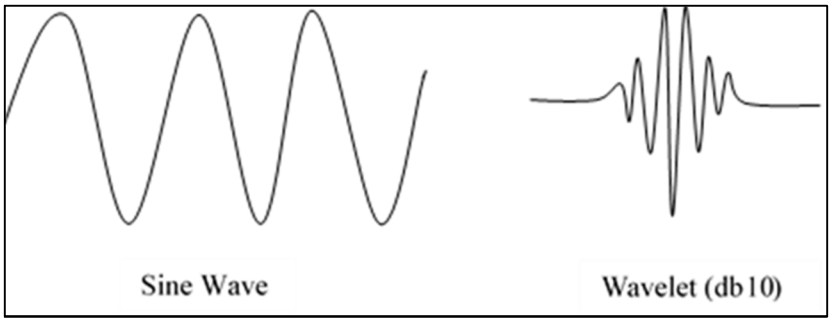

Figure 6.1: Wavelet transformation of sine wave.

In the Fourier analysis, the signals are decomposed into different sine waves. Therefore, irregular wavelet performs better than steady sine for rapidly changing signals as it can give better information about specific and relevant locations. Wavelet analysis can also show any kind of discontinuity, breakdown, trend, noise, coefficient and many more of signals (Misiti et al. 1996). In this study, the wavelet analysis has been done using MATLAB toolbox. There are two types of wavelet analysis which are Discrete wavelet transform and Continuous wavelet transform. There is various subgroup of these two types of wavelet transforms.

6.2.1 **Contentious Wavelet Transform (CWT)**

The continuous wavelet transform (CWT) is a function of the shifted and scaled version of wavelet function Ψ multiplied by the summation over all time of the signal. However, scaling means compressing or stretching the wavelets and scale factor is used to represent the scaling and the wavelet is more compressed when the scale factor is smaller. The wavelet sifting means hastening or detaining its onset.

$$C(position, scale) = \int_{-\infty}^{\infty} f(x)\Psi(position, scale, t)dt \qquad (6.1)$$

Here, C is the wavelet coefficient of CWT as a function of position and scale (Misiti et al. 1996)

6.2.2 **Discrete Wavelet Transform (DWT)**

The Discrete Wavelet transform is a wavelet transform where the wavelets are separately sampled. In this analysis, the original signal is divided into two parts, approximations and details. The approximation *a* is the low pass filter where the low-frequency components of the original signal are separated and the detail *d* is the high pass filter where high-frequency components pass. Moreover, the original signal *x* is not only separated in one level but also the approximation *a* is being decomposed in many lower level (*k=3*) components which are called multiple level decomposition which is shown in Figure 6.2.

The major difference between CWT and DWT is that CWT operates in every scale up to maximum value whereas, in DWT the scale and positions can be preselected and in that way, the size of the analysis reduces its size and become more precise, accurate and fast.

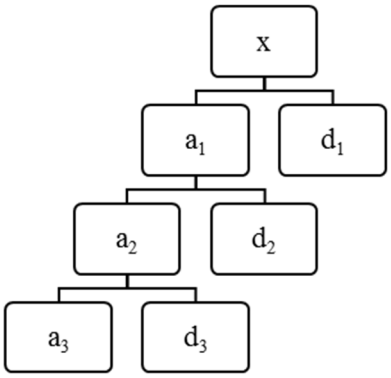

$$x = a_1 + d_1$$
$$= a_2 + d_2 + d_1$$
$$= a_3 + d_3 + d_2 + d_1$$

Figure 6.2: Multiple level Discrete Wavelet analysis.

Mathematically, for j scale and k level the approximate information $f_a^j(x)$ can be can be summation of approximate coefficients $a_{j,k}$ and scale function $\varphi_{j,k}(x)$ as shown in the Equation (6.2). Similarly, the detail information $f_d^j(x)$ can also be described as approximate coefficients $d_{j,k}$ and scale function $\Psi_{jk}(x)$ in the Equation (6.3) below.

$$f_a^j(x) = \sum_k a_{j,k}\varphi_{j,k}(x) \tag{6.2}$$

$$f_d^j(x) = \sum_k d_{j,k}\,\Psi_{jk}(x) \tag{6.3}$$

One of the common way to imply this as logarithmic discretization of the scale s and then connect it to the step size. The step size is the values between the translation parameter τ. The equation is adapted from Gao & Yan (2010) and shown below,

$$\{_{\tau=k\tau_0 s_0^j}^{s=s_0^j} \tau_0 \neq 0;\ s_0 < 1\ (j, k\epsilon Z, where\ Z\ is\ an\ interger) \tag{6.4}$$

$$\Psi_{jk}(x) = s_0^{-0.5j}\Psi(\frac{x}{s_0^j} - k\tau_0) \tag{6.5}$$

$$\Psi_{jk}(x) = 2^{-0.5j}\Psi(\frac{x}{2^j} - k) \tag{6.6}$$

Here, j is the scale and k is the level of the wavelet. Equation (6.5) is the base wavelet equation. Addison (2017) assumed $s_0 = 2$ and $\tau_0 = 1$ therefore the Equation (6.6) can be achieved and finally the discrete wavelet transform will be obtained.

$$W(j,k) = [f(x), \Psi_{jk}(x)] = 2^{-0.5j}\int_{-\infty}^{\infty} f(x)\ \Psi\left(\frac{x}{2^j} - k\right)dx \tag{6.7}$$

$$f(x) = \sum_{j,k} C_{j,k}\Psi_{jk}(x) \tag{6.8}$$

In the Equation (6.7) $f(x)$ is the original signal and in the Equation (6.8) $C_{j,k}$ is the wavelet coefficient. For multilevel wavelet analysis, there are many types of orthogonal wavelet transformation which determines the shape of wavelet. Among them Daubechies Wavelet has been one of most common orthogonal wavelet transformation.

Daubechies Wavelet

Daubechies Wavelet uses scalar products with scaling wavelets and signals to calculate moving average and difference. This method allows obtaining a good range of signal data to compute the average and difference. Daub4 is the most accepted and simple way of analysis wavelets. If we consider a signal *x* constituting *n* number of values, then the daub4 transformation create the mapping $x \overset{D_k}{\rightarrow} (a^k|d^k)$ to its approximation a^k and details d^k sub signal for k-levels.

$$a_m = x.U_m^k \tag{6.9}$$

$$d_m = x.\Psi_m^k \tag{6.10}$$

Where, each value of a_m and d_m are the scaler products. U_m^k is the scaling signal and Ψ_m^k is the wavelet at k-level (Walker 2008).

Wavelet Packet Analysis

In DWT, the main signal is decomposed in approximation and details and the approximation is divided into second level approximation and details and this way n-level of decomposition can be done. In wavelet packet analysis both the details and the approximation can be decomposed which means the signal can be encoded in 2^n ways. The wavelet packet decomposition tree is shown in Figure 6.3.

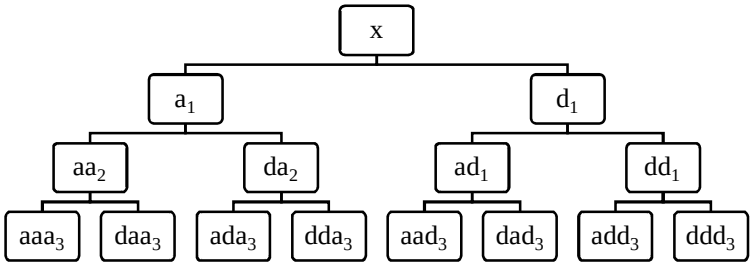

Figure 6.3: Wavelet packet analysis decomposition tree.

In the MATLAB toolbox entropy-based criterion is used to find the most desirable wavelet decomposition. Wavelet packet transformation gives many bases and the best tree based can be found by entropy criterion (Misiti et al. 1996).

Wavelet packets are the general form of orthogonal wavelets. This split up detail spaces to give finer decomposition.

Coifman & Wickerhauser (1992) explained wavelet packet transformation equation as the following.

$$\begin{cases} v_{2i}^{j}(x) = \sqrt{2}\sum_{k} h_k v_i^j(2x-k) \\ v_{2i+1}^{j}(x) = \sqrt{2}\sum_{k} g_k v_i^j(2x-k) \end{cases} ; \; i = 0,1,2,\ldots \; and \; k = 0,1,\ldots m \qquad (6.11)$$

In the above equations, two filters h_k and g_k associated with scaling function $\varphi_{jk}(x)$ and base wavelet function $\Psi_{jk}(x)$ (Gao & Yan 2010).

Wavelet Entropy

Wavelet entropy represents the nonuniformity of states, which is an ideal parameter measure the ordering of unsteady signals (Uyar et al. 2008). It can also give information about the dynamic process and the signal potential. When the coefficient matrix of the wavelet transformation represented by a probability distribution, the calculated wavelet entropy represents randomness of the matrix (Fan et al. 2013). The wavelet packet decomposition is a orthogonal function which means, the total energy entropy of the original signal should be summation of the coefficient energy entropy (Sun et al. 2013). The wavelet entropy energy can be defined as the following Equation (6.12).

$$EN = -\sum_{i=1}^{n} P_i \log P_i \qquad (6.12)$$

Where, $P_i = E_i / \sum_{i=1}^{n} E_i$ is the percentage of coefficient energy of the original signal (Yu et al. 2006).

In this study norm entropy, has been used to analyze the pressure signal. In an orthonormal basis entropy s is the signal s_{ij} is the coefficient of s and E is the entropy function such that $E(0) = 0$ and $E(s) = \sum_i E(s_i)$. This entropy formula is used in MATLAB to calculate norm entropy. The concentration in l^P norm where, $1 \leq P < 2$. Now $E(s) = |s_i|^P$ so $E(s) = \sum_i |s|^P = ||s||_P^P$ for norm entropy method (Misiti et al. 1996). The wavelet entropy can find small or abnormal frequencies. Therefore, wavelet entropy can find different characteristics of multiphase flow.

This study aims to characterize two-phase flow pattern using norm entropy based on wavelet packet decomposition of the pressure signal. This method has follows the steps shown below in the Figure 6.4.

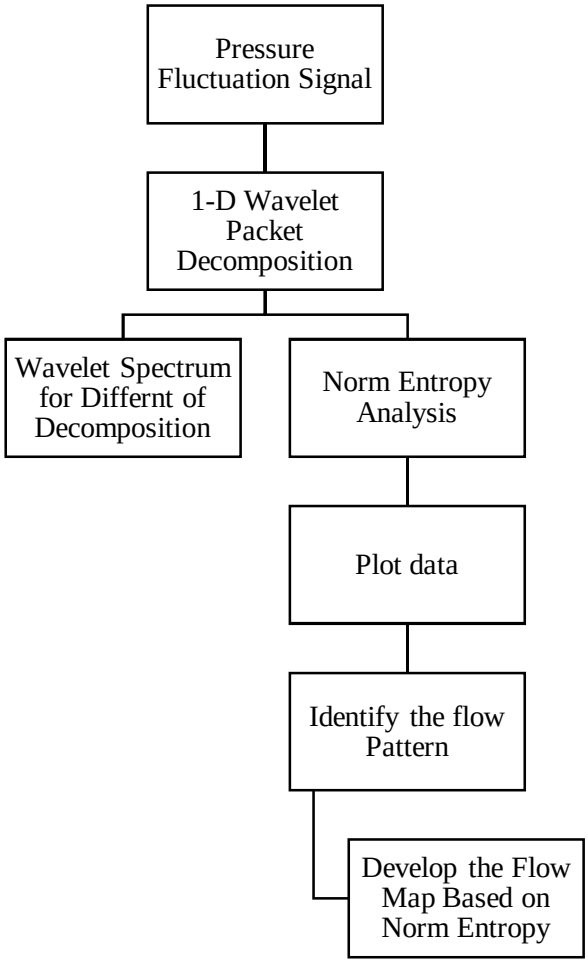

Figure 6.4: The steps of wavelet decomposition for different flow pattern identification.

6.3 Wavelet Packet Analysis of the Experimental Data

In this study, the pressure transducer has given time domain pressure fluctuations which have been analyzed using wavelet packet analysis. As mentioned before this experimental setup only give slug flow and dispersed bubble flow regime and the pressure signal also shows certain characteristics for each kind of flow regimes. The Data acquisition system collected pressure transducer signals with a sampling frequency of 100 Hz. Overall, 10000 data points which were considered to perform wavelet analysis in MATLAB software.

6.3.1 Wavelet Spectrum Analysis

The wavelet packet analysis decomposed the pressure signals into 4-levels. Among the wavelet decomposition method, Daubechies four-scale base wavelet (db4) has been used most frequently in multiphase flow time series decompaction (Shaikh & Al-Dahhan 2007). In this study, Daubechies four-scale base wavelet (db4) and norm entropy analysis method has generated sixteen wavelet packet coefficients. The pressure fluctuation signal achieved from the experimental data only gives 100Hz frequency. So only till 4-level decomposition is enough because the pressure signals do not have high frequency and high-resolution data to get more detailed frequency analysis. The spectrum of the packet wavelet analysis represented the time-frequency plot which provides decomposed frequencies coefficient at a different level. This spectrum represents the time and location of the fluctuation of the signal.

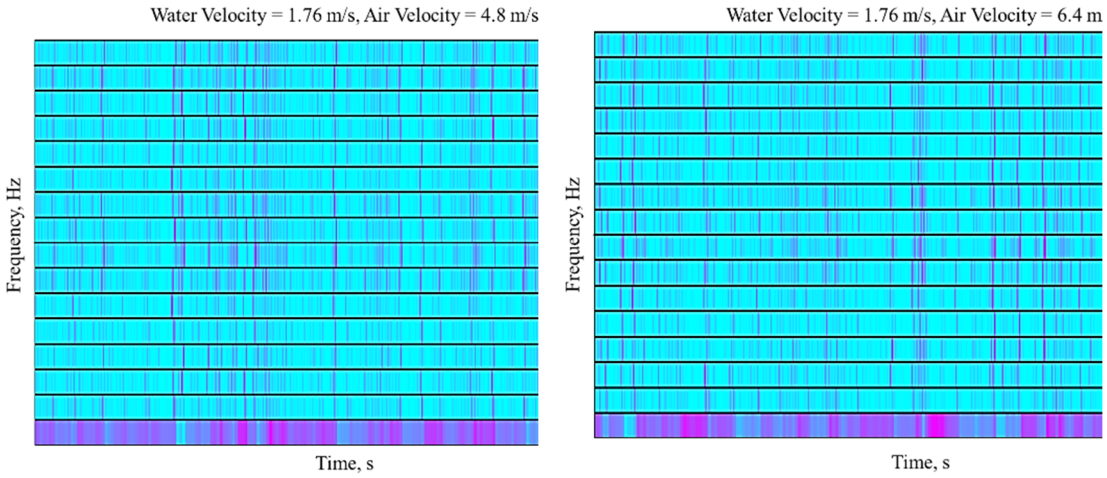

Figure 6.5: Spectrum for Slug flow at different flow condition.

From the Figure 6.5, it can be observed that the time-frequency plot divided the time-frequency plane into concentrated rectangles and this is also a two-dimensional representation of signals. The pink color intensity of each rectangle depends on the coefficient of wavelet packet (Park & Kim 2003).

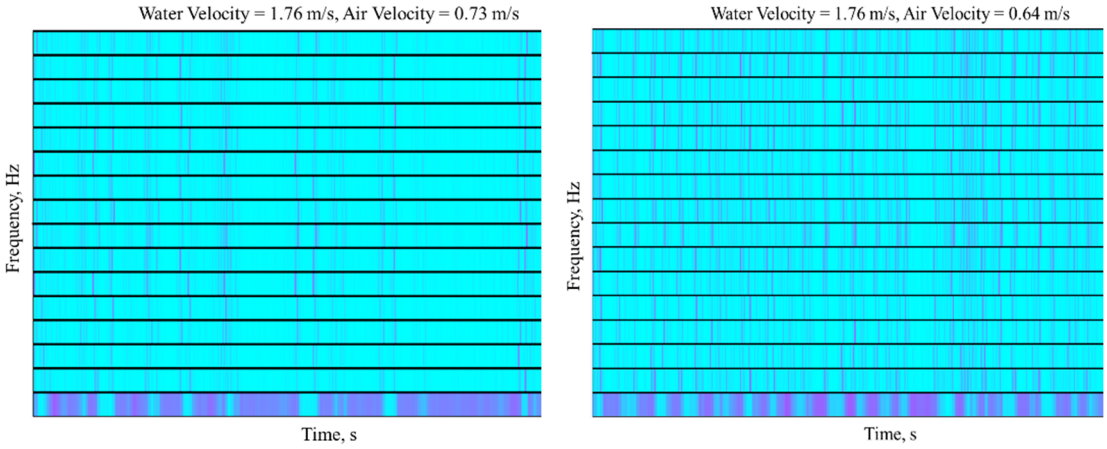

Figure 6.6: Spectrum for bubbly flow in different flow condition.

The similar plot has been observed in Figure 6.6 which is the time-frequency plot for bubbly flow regime for various flow conditions. The intensity of pink shade represents the energy level of a time-frequency cell and lower the energy content the lighter the shade. For the bubbly flow regime, the bubbles are smaller so the pressure fluctuation intensity is less which means low-frequency response has less energy content and the pink shade is light and scattered. In the slug flow the Tylor bubble size is bigger. Therefore, the low-frequency cells have more energy and darker in the shade (Park & Kim 2003). Also, the repetition of the intense pink shade after certain time interval can be an evidence of the picks of the pressure signal. So with a high resolution and better quality sensor where the pressure signal picks are more precise, this map can be a helpful way to understand the flow phenomena inside the pipe. While comparing the wavelet spectrum analysis of bubbly flow and slug flow for the same water flow rate, it has been observed that for bubbly flow the color intensity is comparatively less in the low-frequency response area. However, the use of higher resolution pressure transducer may enhance the wavelet spectrum quality with more precise fluctuation characteristics.

6.3.2 **Wavelet Entropy Analysis**

The wavelet entropy analysis of the pressure fluctuation data represents the nonlinearity of the gas/liquid two-phase flow. After calculating wavelet entropy of 10000 pressure signal data of gas/liquid two-phase horizontal flow, it has been seen that the wavelet entropy increased with the increase of the pressure signal fluctuation.

The entropy values of the pressure fluctuation data have been compared with gas to liquid volume flowrate ratio (GLR) and void fraction ($\alpha_g = \frac{v_g^s}{v_g^s + v_l^s}$). Void fraction is the ratio of gas velocity and mixture velocity.

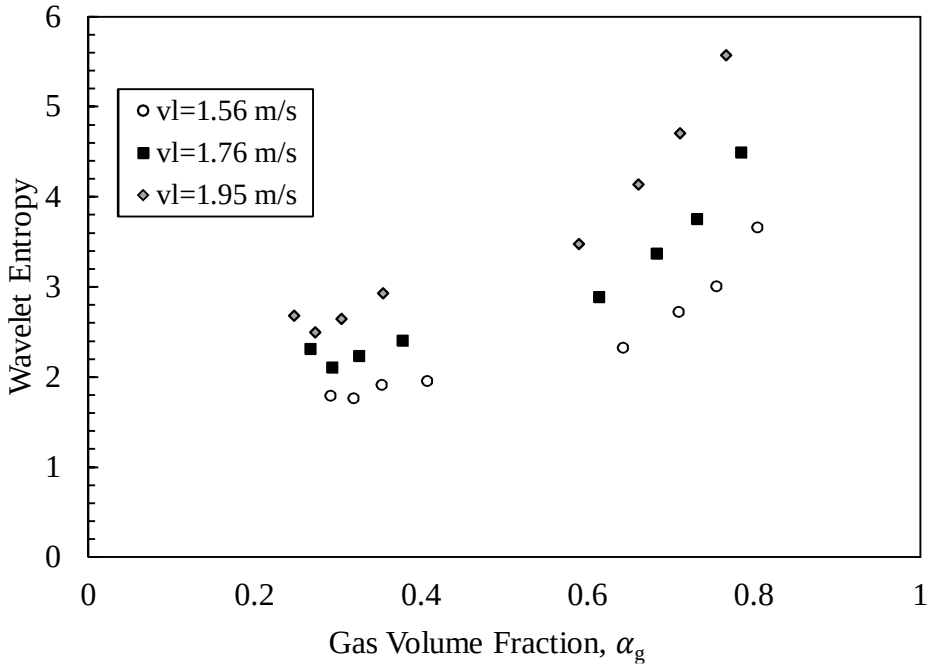

Figure 6.7: Change of wavelet entropy with gas volume fraction for gas/Newtonian fluid.

In Figure 6.7, it has been observed that wavelet entropy increased with the increase of gas void fraction which means the fluctuation of the pressure increases with the increase of void fraction for gas/water flow.

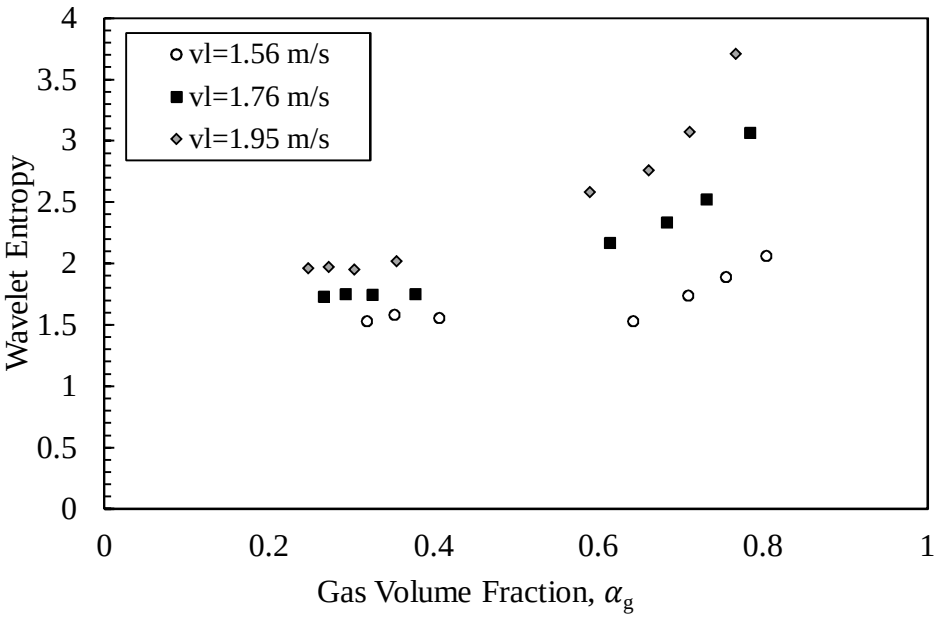

Figure 6.8: Change of wavelet entropy with gas volume fraction for gas/non-Newtonian fluid.

In Figure 6.7, it has been also observed that wavelet entropy increased with the increase of gas void fraction for gas/non-Newtonian fluid. Which means the fluctuation of the pressure increases with the increase of GLR ratio for gas/water flow. Another observation is that the wavelet entropy value for gas/non-Newtonian flow is less than the gas/Newtonian fluid flow. This phenomenon occurred due to the viscosity effect of the non-Newtonian fluid.

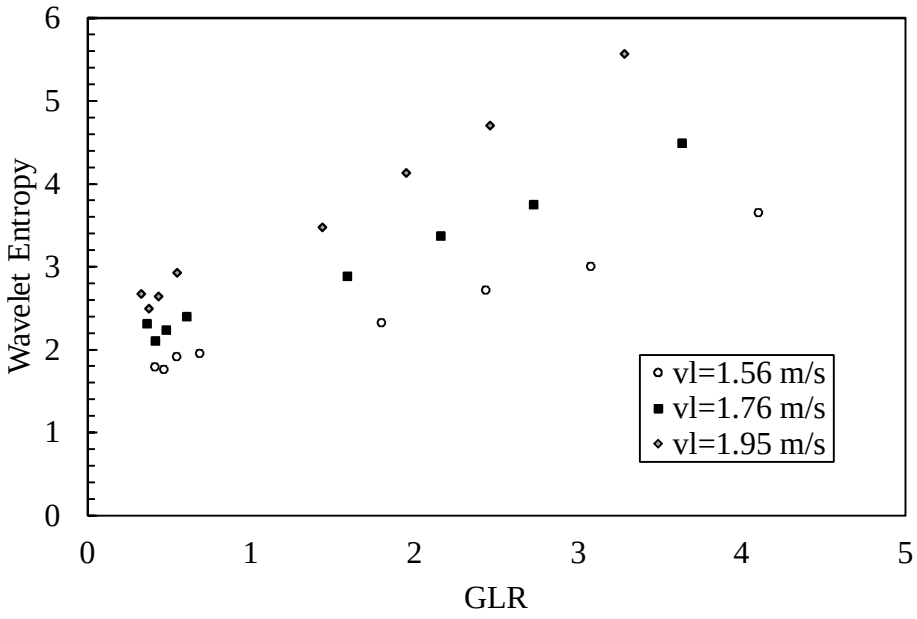

Figure 6.9: Change of wavelet entropy with Gas to Liquid Ratio for gas/Newtonian flow.

In Figure 6.9, it has been observed that the with the growth of GLR ratio the norm wavelet entropy increased which means the fluctuation of the pressure increases with the increase of GLR ratio. However, the norm entropy change at the low GRL is not consistent. Fan et al. (2013) have also seen similar behavior for low GLR ratio and mostly in the bubble flow or bubble-slug transition flow region. As small bubbles motion is random, fast and complicated, it is hard for low-resolution sensor as well as the wavelet norm entropy to detect the pressure signal changes.

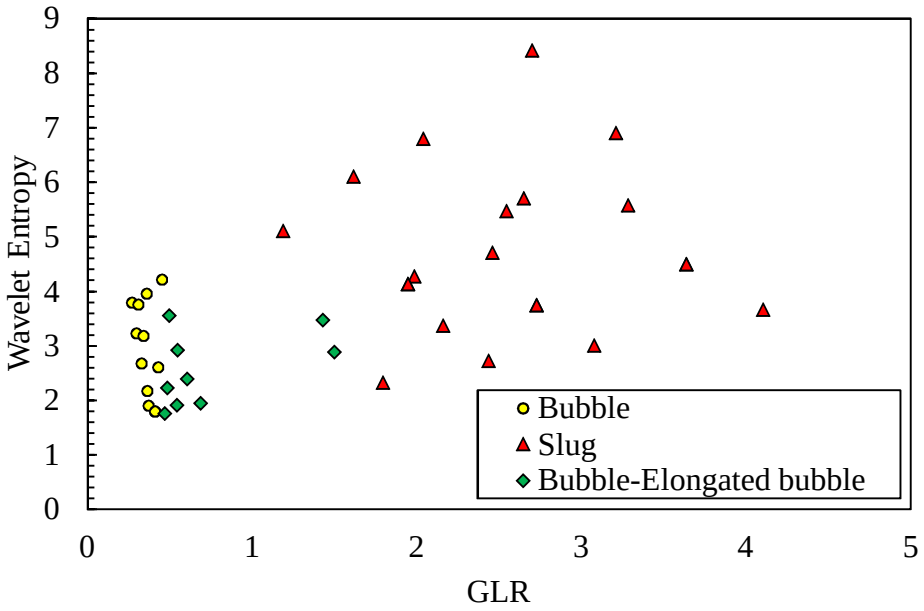

Figure 6.10: Wavelet entropy flow map for gas/Newtonian flow.

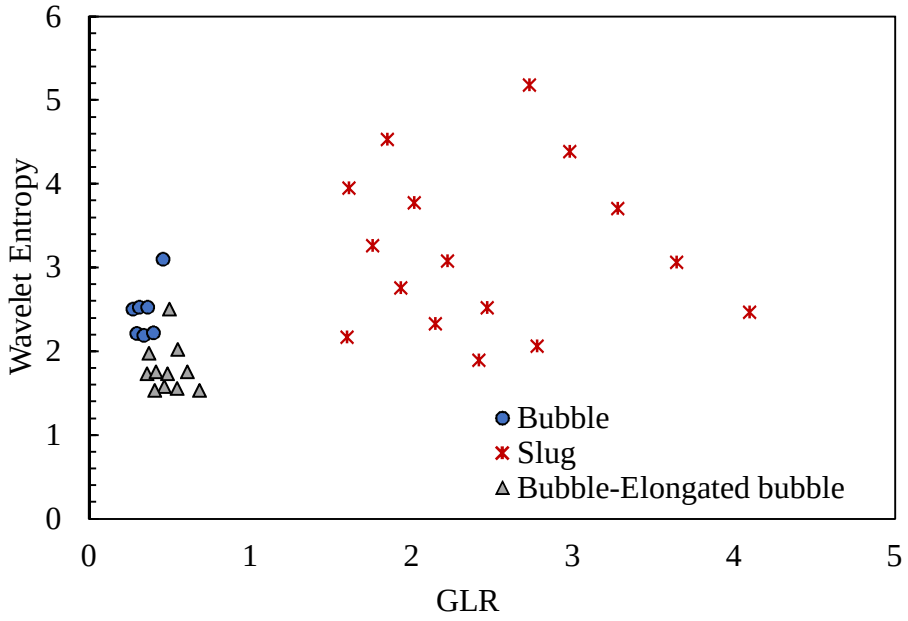

Figure 6.11: Wavelet entropy flow map for gas/non-Newtonian flow.

Figure 6.10 and Figure 6.11 show the wavelet norm entropy of bubble, bubble-elongated bubble and slug flow regime at different GLR of gas/Newtonian and gas/non-Newtonian flow for the experiment setup used in this study. The wavelet norm entropy value may vary with higher resolution sensors. Wavelet norm entropy depends on the pressure fluctuation signal, therefore the more sensitively and precisely the sensor can detect the flow condition the more accurate the wavelet nor entropy will be. However, the wavelet entropy change pattern with a different types of flow regime should remain similar. Fan et al. (2013) and Sun et al. (2013) both got similar wavelet entropy changing pattern but their sensors, experimental setup and experimental condition were different.

6.4 Conclusion

The major objective of this chapter is to analyze the pressure signal fluctuation using wavelet packet transformation to identify the horizontal flow pattern. The wavelet decomposition, and wavelet norm entropy has been given recognizable flow characteristics for bubble, bubble-elongated bubble and slug flow pattern. However, the pressure sensor used in this experiment setup could not give high frequency and high-resolution data and high-resolution sensors can give better and accurate understanding of the flow characteristic. Therefore, 1-D wavelet packet decomposition is a useful method to find different features of multiphase flow and for recognizing different flow patterns.

Chapter 7. Conclusion

In this thesis, the horizontal flow regime maps using experimental data has been developed and validated with the existing literature. In addition, slug frequency has been examined and compared with air/Newtonian and air/non-Newtonian fluid in the flow loop. The slug frequency increase with increased liquid flow rate for both air/water and air/0.1% Xanthan gum solution fluid flow. However, it decreased with increased air flow rate and only for gas/Newtonian fluid slug frequency increase after approximately 5 m/s air velocity. And to form the flow map, this phenomenon can be considered as the starting of the transition zone from slug to Dispersed bubble region. The viscosity effect creates the major difference between gas/water and gas/0.1% Xanthan gum fluid flow. Moreover, pressure signal decomposition has been done for bubble and slug flow using wavelet packet transformation. This signal analysis has successfully identified the signal for different flow pattern and gave different entropy value for various flow pattern pressure signal. However, it can be concluded that the 1-D wavelet packet decomposition can be potential methods to analyze multiphase flow experimental signals and find different characteristics and recognizing different flow patterns.

7.1 Future Recommendation

Multiphase flow analysis has a wide range of research area. The pilot scale experimental setup used in this thesis has the capacity to conduct a different types of multiphase flow analysis. There are some recommendation which should be continued in the future using this setup.

Two-phase vertical and inclined flow maps should be created and verified with the literature. These types of the experiment should be done for air/Newtonian and air/non-Newtonian flow. In this study, only 0.1% Xanthan gum has been used. For non-Newtonian fluid flow analysis, the experiments should be done with higher concentration Xanthan gum solution.

The pump used in this experiment was a centrifugal water pump which cannot handle high viscous fluid with limited flow range. That is why low concentration and low viscous Xanthan gum have been used in this experiment. However, to understand the air/non-Newtonian flow characteristics, using higher viscosity fluid is crucial with higher flow range. Using a screw type progressive cavity pump would be a good replacement of the centrifugal water pump. This is a screw type progressive cavity pump that can handle viscous fluid. It is used to drive drilling fluid which has high viscosity. This pump can provide maximum 1000 kPa discharge pressure and 227 lpm liquid flow rate.

From the previous studies, it has been seen that the pipe diameter influences the flow structure. This experiment has been done in 73.66 mm pipe. Therefore, the experiments

should be done in different diameter pipe to see the ramification of pipe diameter on the flow characteristics.

One of the major future work should be using high resolution and high-frequency pressure sensors to detect the changes of flow structures. The sensors should be utilized around the pipe cross section area so that these could capture every change of multiphase flow. The wavelet packet transformation can identify different pressure fluctuation and it is possible to determine the flow pattern only by seeing the pressure signal.

To conclude, Slug flow analysis and wavelet transform analysis has enormous potential that can be used to understand the multiphase flow. With the integration of recent advanced measurement and visualization technique in this experimental setup, multiphase flow analysis can be taken one step further.

Bibliography

Abed, E.M. & Ghoben, K., 2015. Gas-Liquid Slug Frequency and Slug Unit Length in Horizontal Pipes. *The Iraqi Journal For Mechanical And Material Engineering*, 15.

Addison, P.S., 2017. *The illustrated wavelet transform handbook: introductory theory and applications in science, engineering, medicine and finance*, CRC press.

Al-Safran, E., 2009. Investigation and prediction of slug frequency in gas/liquid horizontal pipe flow. *Journal of Petroleum Science and Engineering*, 69(1), pp.143–155.

Blaney, S., 2008. Gamma radiation methods for clamp-on multiphase flow metering.

Chhabra, R.P. & Richardson, J.F., 1999. *Non-Newtonian Flow: Fundamentals and Engineering Applications*, Butterworth-Heinemann.

Chhabra, R.P. & Richardson, J.F., 1984. Prediction of flow pattern for the co-current flow of gas and non-newtonian liquid in horizontal pipes. *The Canadian Journal of Chemical Engineering*, 62(4), pp.449–454.

Coifman, R.R. & Wickerhauser, M.V., 1992. Entropy-based algorithms for best basis selection. *IEEE Transactions on information theory*, 38(2), pp.713–718.

Ding, H. et al., 2007. Hilbert--Huang transform based signal analysis for the characterization of gas--liquid two-phase flow. *Flow measurement and instrumentation*, 18(1), pp.37–46.

Drahoš, J. et al., 1987. Characterization of hydrodynamic regimes in horizontal two-phase flow: Part II: Analysis of wall pressure fluctuations. *Chemical Engineering and Processing: Process Intensification*, 22(1), pp.45–52.

Dukler, A.E. & Hubbard, M.G., 1975. A model for gas-liquid slug flow in horizontal and near horizontal tubes. *Industrial & Engineering Chemistry Fundamentals*, 14(4), pp.337–347.

Dziubinski, M., Fidos, H. & Sosno, M., 2004. The flow pattern map of a two-phase non-Newtonian liquid--gas flow in the vertical pipe. *International journal of multiphase flow*, 30(6), pp.551–563.

Elperin, T. & Klochko, M., 2002. Flow regime identification in a two-phase flow using wavelet transform. *Experiments in Fluids*, 32(6), pp.674–682.

Fan, C., Ding, Y. & Ren, X., 2013. Wavelet entropy applied in gas-liquid two-phase flow. In *Control Conference (CCC), 2013 32nd Chinese*. pp. 8623–8627.

De Fang, L. et al., 2012. The flow pattern transition identification and interphases force detection of gas-liquid two-phase flow. *AASRI Procedia*, 3, pp.534–539.

Gabor, D., 1946. Theory of communication. Part 1: The analysis of information. *Electrical Engineers-Part III: Radio and Communication Engineering, Journal of the Institution of*, 93(26), pp.429–441.

Gallino, G., Migliori, M. & de Cindio, B., 2001. A rheological approach to drill-in fluids optimization. *Rheologica acta*, 40(2), pp.196–203.

Gao, R.X. & Yan, R., 2010. *Wavelets: Theory and applications for manufacturing*, Springer Science & Business Media.

Gregory, G.A. & Scott, D.S., 1969. Correlation of liquid slug velocity and frequency in horizontal cocurrent gas-liquid slug flow. *AIChE Journal*, 15(6), pp.933–935.

Greskovich, E.J. & Shrier, A.L., 1972. Slug frequency in horizontal gas-liquid slug flow. *Industrial & Engineering Chemistry Process Design and Development*, 11(2), pp.317–318.

Heywood, N.I. & Richardson, J.F., 1978. Head loss reduction by gas injection for highly shear-thinning suspensions in horizontal pipe flow. In *Proc. of Hydrotransport*.

Heywood, N.I. & Richardson, J.F., 1979. Slug flow of air water mixtures in a horizontal pipe: Determination of liquid holdup by γ-ray absorption. *Chemical Engineering Science*, 34(1), pp.17–30.

Hill, T.J., Wood, D.G. & others, 1994. Slug flow: Occurrence, consequences, and prediction. In *University of Tulsa Centennial Petroleum Engineering Symposium*.

Hubbard, M.G., 1965. *An analysis of horizontal gas-liquid slug flow*. University of Houston.

Hubbard, M.G. & Dukler, A.E., 1966. The characterization of flow regimes for horizontal two-phase flow. *Proceedings of the 1996 Heat Transfer and Fluid*, pp.100–121.

Kobzeff, J.M. et al., 2003. Process for clarification of xanthan solutions and xanthan gum produced thereby.

Kouba, G.E. & Jepson, W.P., 1990. The flow of slugs in horizontal, two-phase pipelines. *Journal of Energy Resources Technology*, 112(1), pp.20–24.

Lockhart, R.W. & Martinelli, R.C., 1949. Proposed correlation of data for isothermal two-phase, two-component flow in pipes. *Chem. Eng. Prog*, 45(1), pp.39–48.

Mandhane, J.M. et al., 1975. Critical Evaluation of Holdup Prediction Methods for Gas-Liquid Flow in Horizontal Pipes. *Journal of Petroleum Technology*, 27(08), pp.1–17.

Mandhane, J.M., Gregory, G.A. & Aziz, K., 1974. A flow pattern map for gas-liquid flow in horizontal pipes. *International Journal of Multiphase Flow*, 1(4), pp.537–553.

Misiti, M. et al., 1996. Wavelet toolbox. *The MathWorks Inc., Natick, MA*, 15, p.21.

Otten, L. & Fayed, A.S., 1977. Slug Velocity And Slug Frequency Measurements In Concurrent Air-Non-Newtonian Slug Flow. *Transactions Of The Institution Of Chemical Engineers*, 55(1), pp.64–67.

Park, S.H. & Kim, S.D., 2003. Characterization of pressure signals in a bubble column by wavelet packet transform. *Korean Journal of Chemical Engineering*, 20(1), pp.128–132.

Picchi, D. et al., 2015. Gas/shear-thinning liquid flows through pipes: Modeling and experiments. *International Journal of Multiphase Flow*, 73, pp.217–226.

Rosehart, R.G., Rhodes, E. & Scott, D.S., 1975. Studies of gas liquid (non-Newtonian) slug flow: void fraction meter, void fraction and slug characteristics. *The Chemical Engineering Journal*, 10(1), pp.57–64.

Shaikh, A. & Al-Dahhan, M.H., 2007. A review on flow regime transition in bubble columns. *International Journal of Chemical Reactor Engineering*, 5(1).

Shea, R. et al., 2004. Slug frequency prediction method comparison. In *Proceedings of the 4th North American Conference on Multiphase Technology*. pp. 227–237.

Sun, Z., Shao, S. & Gong, H., 2013. Gas--liquid Flow Pattern Recognition Based on Wavelet Packet Energy Entropy of Vortex-induced Pressure Fluctuation. *Measurement science review*, 13(2), pp.83–88.

Taitel, Y. & Dukler, A.E., 1976. A model for predicting flow regime transitions in horizontal and near horizontal gas-liquid flow. *AIChE Journal*, 22(1), pp.47–55.

Tutu, N.K., 1982. Pressure fluctuations and flow pattern recognition in vertical two phase gas-liquid flows. *International Journal of Multiphase Flow*, 8(4), pp.443–447.

Uyar, M., Yildirim, S. & Gencoglu, M.T., 2008. An effective wavelet-based feature extraction method for classification of power quality disturbance signals. *Electric Power Systems Research*, 78(10), pp.1747–1755.

Walker, J.S., 2008. *A primer on wavelets and their scientific applications*, CRC press.

Yu, Y., Junsheng, C. & others, 2006. A roller bearing fault diagnosis method based on EMD energy entropy and ANN. *Journal of sound and vibration*, 294(1), pp.269–277.

Zabaras, G.J., 1999. Prediction of slug frequency for gas-liquid flows. In *SPE Annual Technical Conference and Exhibition*.

Zabaras, G.J., Shell, E. & Co, P.T., 2000. Prediction of Slug Frequency for Gas / Liquid Flows. , (September), pp.252–258.